ARTICLE OPEN

Check for updates

Cancer associated fibroblasts serve as an ovarian cancer stem cell niche through noncanonical Wnt5a signaling

Yiming Fang[1,2], Xue Xiao[1,2], Ji Wang[1,2], Subramanyam Dasari[1,2], David Pepin[3], Kenneth P. Nephew[1,2], Dmitriy Zamarin[4] and Anirban K. Mitra[1,2]✉

Frequent relapse and chemoresistance cause poor outcome in ovarian cancer (OC) and cancer stem cells (CSCs) are important contributors. While most studies focus exclusively on CSCs, the role of the microenvironment in providing optimal conditions to maintain their tumor-initiating potential remains poorly understood. Cancer associated fibroblasts (CAFs) are a major constituent of the OC tumor microenvironment and we show that CAFs and CSCs are enriched following chemotherapy in patient tumors. CAFs significantly increase OC cell resistance to carboplatin. Using heterotypic CAF-OC cocultures and in vivo limiting dilution assay, we confirm that the CAFs act by enriching the CSC population. CAFs increase the symmetric division of CSCs as well as the dedifferentiation of bulk OC cells into CSCs. The effect of CAFs is limited to OC cells in their immediate neighborhood, which can be prevented by inhibiting Wnt. Analysis of single cell RNA-seq data from OC patients reveal Wnt5a as the highest expressed Wnt in CAFs and that certain subpopulations of CAFs express higher levels of Wnt5a. Our findings demonstrate that Wnt5a from CAFs activate a noncanonical Wnt signaling pathway involving the ROR2/PKC/CREB1 axis in the neighboring CSCs. While canonical Wnt signaling is found to be predominant in interactions between cancer cells in patients, non-canonical Wnt pathway is activated by the CAF-OC crosstalk. Treatment with a Wnt5a inhibitor sensitizes tumors to carboplatin in vivo. Together, our results demonstrate a novel mechanism of CSC maintenance by signals from the microenvironmental CAFs, which can be targeted to treat OC chemoresistance and relapse.

npj Precision Oncology (2024)8:7 ; https://doi.org/10.1038/s41698-023-00495-5

INTRODUCTION

Ovarian cancer (OC) is the deadliest gynecologic malignancy and the fifth leading cause of cancer-related deaths among women in the USA[1]. Cytoreductive surgery combined with carbo-taxol chemotherapy is the current standard of care, but most patients eventually relapse and develop chemoresistance[2,3]. The emergence of chemoresistance is a complicated process and several reports suggest that cancer stem cells (CSCs) or tumor-initiating cells are responsible for the development of OC chemoresistance[4,5]. Moreover, accumulating evidence has implicated the contribution of the tumor microenvironment (TME) in chemoresistance and relapse[6,7]. However, the relationship between the TME and CSCs in the context of chemoresistance/recurrence and the underlying regulatory mechanisms are not very well understood.

Most cancers comprise a heterogeneous population of cells, and CSCs are a distinct subpopulation that was identified in several hematologic and solid tumors[8]. CSCs can undergo symmetric division for self-renewal and divide asymmetrically to give rise to progenies that differentiate to contribute to the heterogeneity in the tumor[9]. The CSC population may also be maintained by dedifferentiation of certain non-CSCs[10]. The chemoresistance of CSCs is believed to be caused by increased DNA repair, efflux of toxins, anti-apoptotic genes, and entering a quiescent state[11]. Following chemotherapy, CSCs survive and are enriched in the residual tumors, which eventually cause recurrence[12].

The stem cell niche refers to cellular and acellular components surrounding the stem cells in normal tissues that provide an optimal microenvironment and regulate their fate. The cancer stem cell niche can consist of TME components like cancer-associated fibroblasts (CAFs), inflammatory cells, mesenchymal stem cells, extracellular matrix, and cytokines, which provide a suitable microenvironment for CSCs[13,14]. CSCs share pathways for self-renewal with normal stem cells, like Wnt, Sonic Hedgehog, and Notch, providing potential targets for eliminating CSCs. As the predominant cell type in the tumor stroma, CAFs are primarily responsible for synthesizing and remodeling the extracellular matrix surrounding the CSCs and provide signals that initiate or enhance tumor progression[15–17]. During chemotherapy, CAFs protect CSCs in multiple ways. By releasing growth factors, CAFs can activate various survival signaling pathways in CSCs, which help them resist DNA damage[18]. CAFs also reduce CSCs uptake of therapeutic drugs by increasing the interstitial fluid pressure[19]. In addition, CAFs promote the epithelial-to-mesenchymal transition of CSCs, which increases the self-renewal of CSCs[20].

We investigated the role of CAFs in providing a supportive microenvironment for OC stem cells (OCSCs) in high-grade serous OC (HGSOC), the most common and lethal OC subtype. Here, we report how CAFs serve as an OCSC niche, causing relapse and chemoresistance. We demonstrate that CAFs signal to proximal OC cells via Wnt5a, inducing a non-canonical Wnt signaling pathway in the cancer cells, causing self-renewal of OCSCs and dedifferentiation of some non-OCSCs into OCSCs.

[1]Indiana University School of Medicine-Bloomington, Indiana University, Bloomington, IN, USA. [2]Indiana University Simon Comprehensive Cancer Center, Indiana University School of Medicine, Indianapolis, IN, USA. [3]Pediatric Surgical Research Laboratories, Massachusetts General Hospital; Department of Surgery, Harvard Medical School, Boston, MA, USA. [4]Department of Medicine, Memorial Sloan Kettering Cancer Center, New York, NY, USA. ✉email: anmitra@indiana.edu

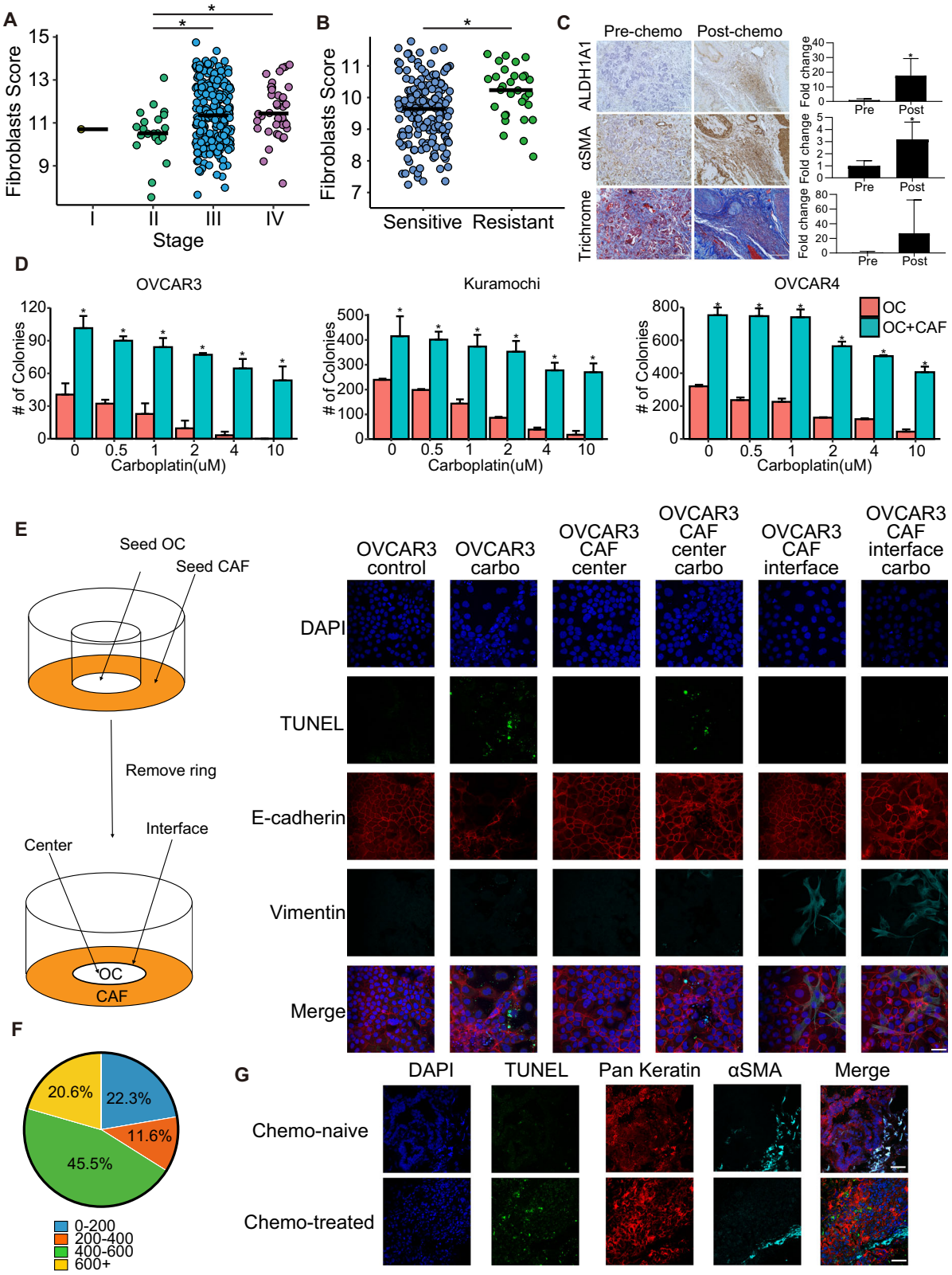

RESULTS

CAFs are associated with chemoresistance

The presence of a higher proportion of stroma in tumors has been implicated to result in poor response to chemotherapy in OC[21]. Moreover, neoadjuvant chemotherapy can cause fibrosis in the residual lesions[22,23]. Therefore, we performed a deconvolution analysis of TCGA OC data to test the effect of tumor stage on the fibroblast score (Fig. 1A). The fibroblast score was determined using MCP-counter Version 1.2.0, which utilizes a set of fibroblast markers (Supplementary Fig. 1A) and was found to increase with

Fig. 1 CAFs and OC chemoresistance. A The Cancer Genome Atlas (TCGA) ovarian cancer data contain both clinical and gene expression profiles from patient samples. Microenvironment Cell Populations-counter (MCP-counter, version 1.2.0) was applied to deconvolve fibroblasts in TCGA dataset. MCP-counter produced abundance scores for each cell type based on marker genes detected. The fibroblast abundance score is plotted for each stage. Data from 305 ovarian cancer patients, bar depicts median, $*p < 0.005$ (*t*-test). **B** The Australian Ovarian Cancer Study (AOCS) dataset (GSE9891) profiled gene expression of 285 ovarian patient samples, segregated into chemo-resistant and chemo-sensitive. Deconvolution analysis of the AOCS dataset was done using MCP-counter version 1.2.0. The fibroblast scores for sensitive and resistant patients was plotted. Data from 284 ovarian cancer patients, bar depicts median, $*p < 0.005$ (*t*-test). **C** Representative immunohistochemical staining for ALDH1A1 (OCSC marker), αSMA (CAF marker), and Masson's trichrome staining in HGSOC patient omental metastasis pre- and post-chemotherapy (matched) (Scale bar: 200 μm). The staining for ALDH1A1 and αSMA, and the ratio of pink/blue for trichrome from 7 matched pre- and post-chemotherapy patient specimens were quantified and plotted (Right). $*p < 0.05$ (paired t-test). **D** Three different HGSOC cell lines (OVCAR3, Kuramochi, OVCAR4) were seeded in 6-well plates with/without CAFs and allowed to form colonies and treated with increasing doses of carboplatin. Colonies were fixed, stained, and manually counted and quantified using ImageJ. Mean ± SD from three independent experiments. $*p < 0.01$ (*t*-test). **E** Interface interaction assay of OVCAR3 cocultured with CAFs. OVCAR3 cells and CAFs were seeded on 10 mm coverslip separated by cloning ring. The ring was removed after 24 h and cells were allowed to grow and merge at the interface followed by carboplatin treatment (33 μM). TUNEL assay was done to label apoptotic cells (green). Cancer cells and CAFs were stained with E-cadherin (red) and vimentin (teal) respectively. *Left:* Schematic outline of the assay setup. *Right:* Images of immunofluorescence staining of cocultures (Leica SP8, 40x objective). Scale bar: 50 μm. **F** The distance (μm) between apoptotic OVCAR3 cells and nearest CAFs in the interface interaction assay was measured by ImageJ and plotted as % of apoptotic cells at increasing distances from CAFs. 600+ μm is close to the periphery of the imaging field and had fewer cells. **G** Immunofluorescent staining of pre- and post-chemotherapy OC patient tumors. TUNEL assay was used to label apoptotic cells and immunofluorescence staining was done to label cancer cells (pan-keratin) and CAFs (αSMA). Scale bar: 200 μm.

the tumor stage. A reactive stroma signature had been demonstrated to result in poor OC survival[24]. Our deconvolution analysis of that gene expression data further demonstrated that the fibroblast score was higher in the chemoresistant patients in that dataset (Fig. 1B and Supplementary Fig. 1B). Since it has been reported that CSCs are resistant to chemotherapy, we tested the expression levels of ALDH1A1, a standard marker for OCSCs, in matched pre- and post-chemotherapy omental metastasis from 7 OC patients (Fig. 1C and Supplementary Fig. 2). A marked increase in ALDH1A1 expression was observed in the post-chemotherapy specimen. Similarly, α-smooth muscle actin (αSMA) expression was higher in the post-chemotherapy specimen, indicating the enrichment of CAFs (Fig. 1C and Supplementary Fig. 2). Masson's trichrome staining did not show a significant difference in the ratio of cytoplasm to collagen (Fig. 1C and Supplementary Fig. 2). To experimentally test the effect of CAFs on OC chemoresistance, we performed colony formation assay with or without CAFs and treated them with increasing concentrations of carboplatin. The CAFs used in these and subsequent experiments were isolated from HGSOC tumors and immortalized with human telomerase reverse transcriptase unless specified. CAFs were confirmed to express αSMA and vimentin while lacking the expression of keratin (Supplementary Fig. 3A). The presence of CAFs significantly protected the OC cells from carboplatin (Fig. 1D and Supplementary Fig. 3B, C). It is important to understand if this protective effect was limited to OC cells in proximity to CAFs or could also be extended to OC cells further away. To address this, we designed an experimental setup, which we call interface interaction assay, where OC cells were seeded in the center and CAFs in the periphery, with a defined interface where the two cells were in direct contact (Fig. 1E). The cells were then treated with carboplatin and its effect on apoptosis was observed using terminal deoxynucleotidyl transferase dUTP nick end labeling (TUNEL). OVCAR3 cells were stained with E-cadherin as they are very epithelial with high expression of E-cadherin and do not express vimentin (Supplementary Fig. 3A). CAFs were labeled with vimentin. Carboplatin-induced apoptosis in OC cells growing alone and in OC cells growing further away from CAFs, while the OC cells near the CAFs were protected (Fig. 1E and Supplementary Fig. 3D). A higher percentage of apoptotic OC cells were found at a distance >400 μm from the CAFs (Fig. 1F). This was further confirmed in tumors from OC patients. Chemotherapy-treated patient tumors had a higher rate of apoptosis and cancer cells in proximity of CAFs were protected (Fig. 1G). Cancer cells were labeled with pan keratin and CAFs with αSMA. These results indicate that CAFs protect OC cells in their vicinity from chemotherapy.

CAFs induce OCSCs

Since CSCs are more resistant to chemotherapy and both CSCs and CAFs are enriched in post-chemotherapy patients (Fig. 1C), we studied the possible role of CAFs in regulating OCSCs. Coculturing CAFs with OC cells increased the number of OCSCs (Schematic outline in Supplementary Fig. 4A), as evidenced by an increase in the number of $ALDH^+$ cells in the OC population (non-RFP) evaluated by immunofluorescence (IF) imaging (Fig. 2A, Supplementary Fig. 4B). This was separately confirmed by labeling the OC cells with E-cadherin, CAFs with vimentin and assessing ALDH1 expression in the coculture compared to OC monoculture (Supplementary Fig. 4C). Flow cytometric analysis following ALDEFLUOR assay in cocultured OC and RFP-CAFs was done to quantify the fraction of OC cells that were $ALDH^+$ (Fig. 2B, Supplementary Figs. 4D and 11). The increase in $ALDH^+$ OCSCs were further confirmed by performing flow cytometric analysis of ALDEFLUOR assay done in cocultures of RFP expressing OVCAR3 cells with normal CAFs. The fraction of RFP cells exhibiting green fluorescence was quantified (Supplementary Fig. 4E). OVCAR3 cells isolated by fluorescence-activated cell sorting (FACS) after coculturing with RFP expressing CAFs had increased expression of ALDH1 (Supplementary Fig. 5A). Freshly isolated, non-immortalized CAFs had a similar effect in inducing ALDH activity in OC cells (Supplementary Fig. 5B). Similarly, coculture with CAFs increased spheroid formation in ultra-low adhesion plates, indicating an induction of OCSCs (Fig. 2C). The gold standard for evaluating CSCs is the in vivo limiting dilution assay. Therefore, to confirm our results, we performed an in vivo limiting dilution assay using OVCAR3 cells cocultured with RFP expressing CAFs for 7 days, then isolated using FACS and injected subcutaneously into the right flank of mice. The left flank was injected with sham treated OVCAR3 cells (Fig. 2D). The pre-coculture with CAFs increased the tumor-initiating cell frequency 10-fold, with an increase in ALDH1A1 expression in the pre-cocultured tumors, further confirming the role of CAFs in inducing OCSCs (Fig. 2D, E). Having performed the previous studies with OC cell lines, we tested the effect of CAFs on primary OC cells derived from HGSOC patient ascites. As with OC cell lines, the coculture of patient-derived OC cells with CAFs increased $ALDH^+$ cells and spheroid formation (Fig. 2F, G, Supplementary Fig. 11). Having demonstrated that CAFs can induce OCSCs, we next studied if this is through increased symmetric division of OCSCs or by potential

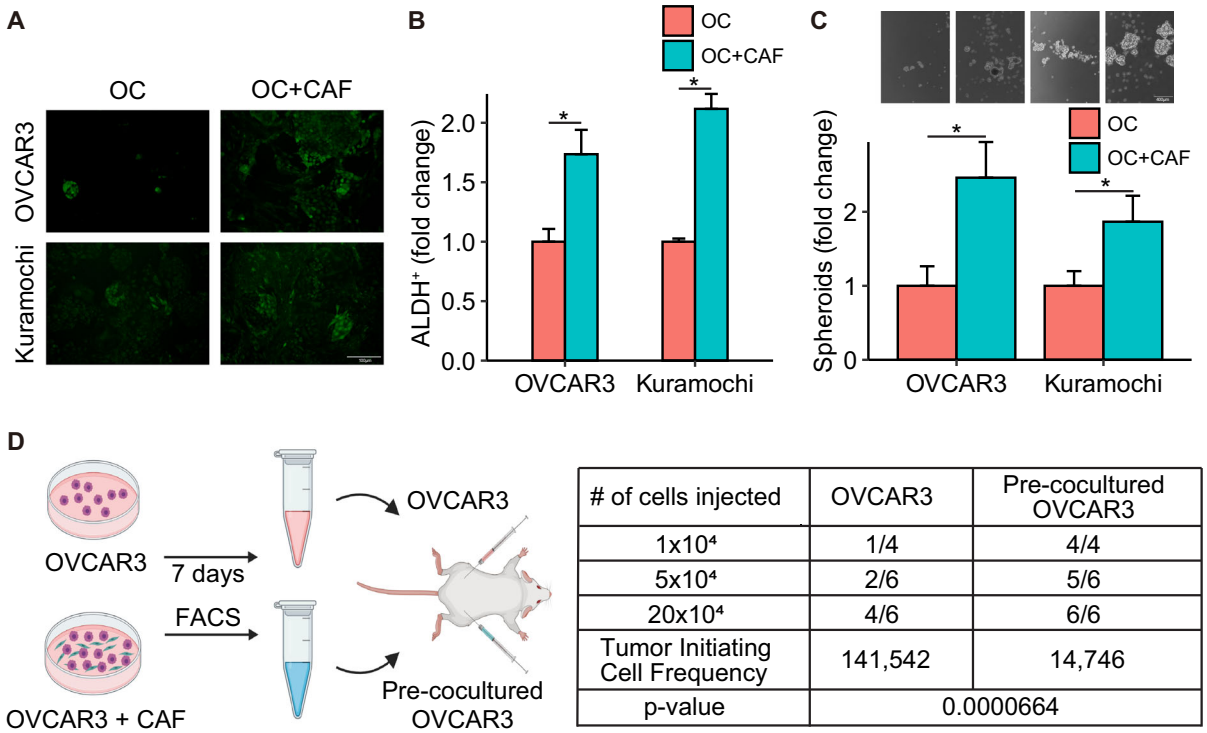

# of cells injected	OVCAR3	Pre-cocultured OVCAR3
1x10⁴	1/4	4/4
5x10⁴	2/6	5/6
20x10⁴	4/6	6/6
Tumor Initiating Cell Frequency	141,542	14,746
p-value	0.0000664	

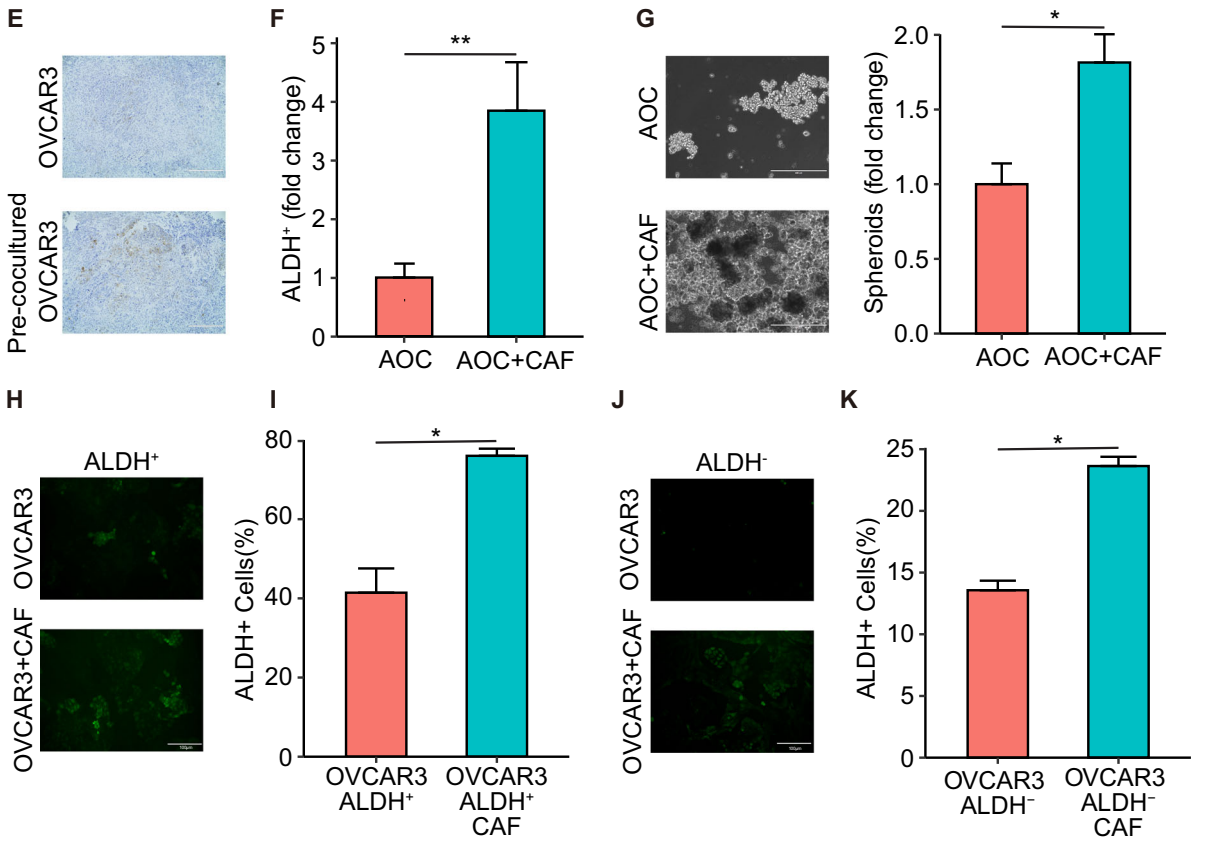

dedifferentiation of some differentiated OC cells. The latter mechanism is observed when non-cancer stem cells are grown for a period, they eventually restore the homeostatic levels of CSCs[25]. To test the possible mechanisms, OVCAR3 cells were first sorted in ALDH⁺ and ALDH⁻ populations followed by coculture with CAFs. CAFs could help sustain a high ALDH⁺ population of OVCAR3 cells (Fig. 2H, I, Supplementary Fig. 11), while also inducing ALDH⁺ cells rapidly in the ALDH⁻ OVCAR3 cells (Fig. 2J, K, Supplementary Fig. 11). This can indicate that CAFs potentially induce stemness in OC cells, by increasing symmetric division of

Fig. 2 CAFs regulate OCSCs. A, **B** ALDEFLUOR assay for stem cell enrichment in OC-CAF coculture. OVCAR3/Kuramochi cells were seeded with CAFs and cocultured for a week. ALDEFLUOR assay was performed to label CSC (green). **A** Fluorescent imaging of OC-CAF coculture labeled by ALDEFLUOR. Scale bar: 100 μm. **B** Flow cytometry analysis was done to quantify CSCs in control/CAF cocultured group. Mean ± SD from three independent experiments. *$p < 0.01$ (*t*-test). **C** Spheroid formation assay of OC-CAF coculture. OVCAR3/Kuramochi cells were seeded with/without CAFs in ultra-low adhesion plates and cocultured for 14 days. Images and quantification of number of spheroids are shown as fold change compared to the respective OC cell alone. Scale bar: 400 μm. Mean ± SD from three independent experiments. *$p < 0.01$ (*t*-test). **D**, **E** Limiting dilution assay for tumor initiation frequency. OVCAR3 cells were cocultured with RFP expressing CAFs for 7 days, followed by isolation using FACS, then subcutaneously injected into the right flank of female NSG mice. Control, sham treated OVCAR3 cells were injected into the left flank of the same mouse. **D** Schematic of the experiment plan (left) and the tumor formation and tumor-initiating cell frequency calculated by extreme limiting dilution analysis (ELDA) are shown (right). **E** Representative IHC Images of the xenograft tumor sections stained with ALDH1A1. Scale bar: 400 μm. **F** ALDEFLUOR assay for stem cell enrichment in OC-CAF coculture using OC patient derived ascites cells. Ascites derived ovarian cancer (AOC) cells were seeded with/without CAFs and cocultured for a week. ALDEFLUOR assay was performed to label CSC (green). Flow cytometry analysis was done to quantify CSCs in control/CAF cocultured groups. Mean ± SD from three independent experiments. **$p < 0.05$ (t-test). **G** Spheroid formation assay using AOCs. AOCs were seeded with/without CAFs in ultra-low adhesion plates and cocultured for 14 days. Images and quantifications are shown. Scale bar: 400 μm. Mean ± SD from three independent experiments. *$p < 0.01$ (*t*-test). **H**–**K** ALDEFLUOR assay of OC-CAF coculture for stem cell enrichment using pure CSC/non-CSC. Following ALDEFLUOR assay, the OVCAR3 cells were sorted by FACS to isolate pure $ALDH^+$ and $ALDH^-$ cells. The $ALDH^+$ and $ALDH^-$ cells were then seeded with CAFs and cocultured for a week. ALDEFLUOR assay was again performed to label CSC (green). Fluorescent imaging (**H**, **J**) and flow cytometric analysis (**I**, **K**) of $ALDH^+$ (**H**–**I**) and $ALDH^-$ (**J**, **K**) were shown. Scale bar: 100 μm. Mean ± SD from three independent experiments. *$p < 0.01$ (*t*-test).

OCSCs or by preventing their differentiation to maintain their population, and by causing dedifferentiation of some differentiated OC cells back into OCSCs.

CAFs induce OCSCs through Wnt5a

Our previous data indicated that CAFs afforded protection to proximal OC cells from carboplatin-induced apoptosis (Fig. 1E–G). We next tested the effect of CAFs on OCSC induction in proximal vs. distal OC cells using the same experimental setup. A high number of $ALDH^+$ cells were observed in OC cells in proximity of CAFs compared to OC cells further away (Fig. 3A, Supplementary Fig. 6A). Moreover, conditioned medium from CAFs failed to induce OCSCs (Supplementary Fig. 6B). Taken together, this indicates the potential role of a juxtacrine signaling mechanism or the involvement of insoluble secreted factors that do not travel longer distances. Therefore, we focused on such factors among the heterotypic signaling mechanisms that have been reported to play a role in CSC[26]. NOTCH and Wnt signaling fit this criterion. Treatment with a NOTCH inhibitor in CAF-OC coculture did not inhibit OCSCs (Supplementary Fig. 6C), however, treatment with a Wnt inhibitor resulted in inhibition of $ALDH^+$ OC cells and spheroid formation in ultra-low adhesion plates (Fig. 3B, C, Supplementary Figs. 6D, 7A, and 11). The Wnt inhibitor IWP2 inhibits porcupine O-acyltransferase (PORCN), which is involved in Wnt processing in the endoplasmic reticulum. IWP2 treatment inhibited both CAF and OC cells PORCN in the cocultures. To identify the specific contribution of CAF and OC-derived Wnt, PORCN was silenced in either CAFs or OVCAR3 cells or both followed by coculture (Supplementary Fig. 7B). While silencing PORCN in OVCAR3 cells had no effect on $ALDH^+$ cells, silencing it in CAFs significantly reduced OCSCs, which was not significantly different from the effect of silencing PORCN in both CAFs and OVCAR3 cells (Fig. 3D, Supplementary Fig. 7C). Next, we analyzed single-cell RNA-seq (scRNA-seq) data from 11 HGSOC patients[27] to identify the potential Wnt involved. Wnt5a was the most highly expressed Wnt in the tumor fibroblasts (Fig. 3E). Further analysis of the subpopulations of tumor fibroblasts (Fig. 3F, FB0-FB8) revealed a marked heterogeneity in them in relation to Wnt5a expression (Fig. 3G and Supplementary Fig. 7D). The subpopulation FB2 had the highest while FB8 had the lowest Wnt5a expression. To further confirm these findings, we used CAFs, OVCAR3, and Kuramochi cells to determine the baseline expression of a panel of Wnts reported to play a role in CAF-OC crosstalk involved in CSCs[28–33] and are expressed more in OC CAFs compared to normal omental fibroblasts[17]. CAFs clearly expressed higher amounts of Wnts than OC cells, with Wnt5a being the most highly expressed (Fig. 3H). Interestingly, the coculture of CAFs with OVCAR3 or Kuramochi cells further induced Wnt5a expression, indicating a potential reciprocal signaling mechanism (Fig. 3I). A comparison of a panel of CAFs isolated from OC patient tumors and a panel of patient-derived normal omental fibroblasts indicated that CAFs have higher expression of Wnt5a (Supplementary Fig. 7E). Treatment with carboplatin further induced Wnt5a expression in CAFs (Fig. 3J, Supplementary Fig. 12). Moreover, analysis of the Australian Ovarian Cancer Study data indicated that high expression of WNT5A resulted in a significantly higher expression of CSC markers (Fig. 3K and Supplementary Fig. 8A). Disease-free survival (DFS) analysis in OC patients using OVMARK database[34], selecting for median survival and for patients who received chemotherapy, indicated that high WNT5A expression resulted in a significant decrease in DFS (Hazard ratio = 12.02 on 1df, p = 0.0005253) (Fig. 3L). Since early relapse is an indicator of chemoresistance, in our analysis, DFS is an effective measurement of the contribution of WNT5A towards drug tolerance in OC patients receiving chemotherapy.

Having identified Wnt5a as a key factor secreted by CAFs, which has potential clinical significance, we studied its role in maintaining OCSCs. Treatment of CAF-OVCAR3 cocultures with a Wnt5a-specific inhibitor, Box5, abrogated OCSC induction (Fig. 4A–C, Supplementary Fig. 11). Box5 (Millipore Sigma, Cat. No. 681673) is a Wnt5a derived hexapeptide that selectively and competitively inhibits Wnt5a binding to its receptor. Furthermore, knocking out Wnt5a in CAFs resulted in the loss of OCSC induction in the cocultures (Fig. 4D and Supplementary Fig. 8B). Treatment of OVCAR3 cells with Box5 caused a decrease in ALDH1A1, SOX2, OCT4 and NANOG expression (Fig. 4E). Confocal immunofluorescence imaging of 3D heterotypic cocultures consisting of CAFs and OVCAR3 cells demonstrated increased ALDH1 expression in OVCAR3 cells in the vicinity of CAFs that expressed Wnt5a (Fig. 4F, Supplementary Fig. 8C).

Wnt5a signals through a non-canonical Wnt signaling pathway to induce OCSCs

Wnt5a can inhibit canonical Wnt signaling or induce non-canonical Wnt signaling in the target cells[35]. Therefore, we analyzed the 11 HGSOC patient scRNA-seq data[27] using CellChat v1.5.0[36], to determine if the CAF-OC crosstalk induces canonical or non-canonical Wnt signaling. Interestingly, canonical Wnt signaling involved only the cancer cell subpopulations (Fig. 5A, CC0-12), where they could interact in a paracrine or autocrine manner. The noncanonical Wnt signaling was predominant in the crosstalk between CAFs and cancer cell subpopulations, where CAFs were

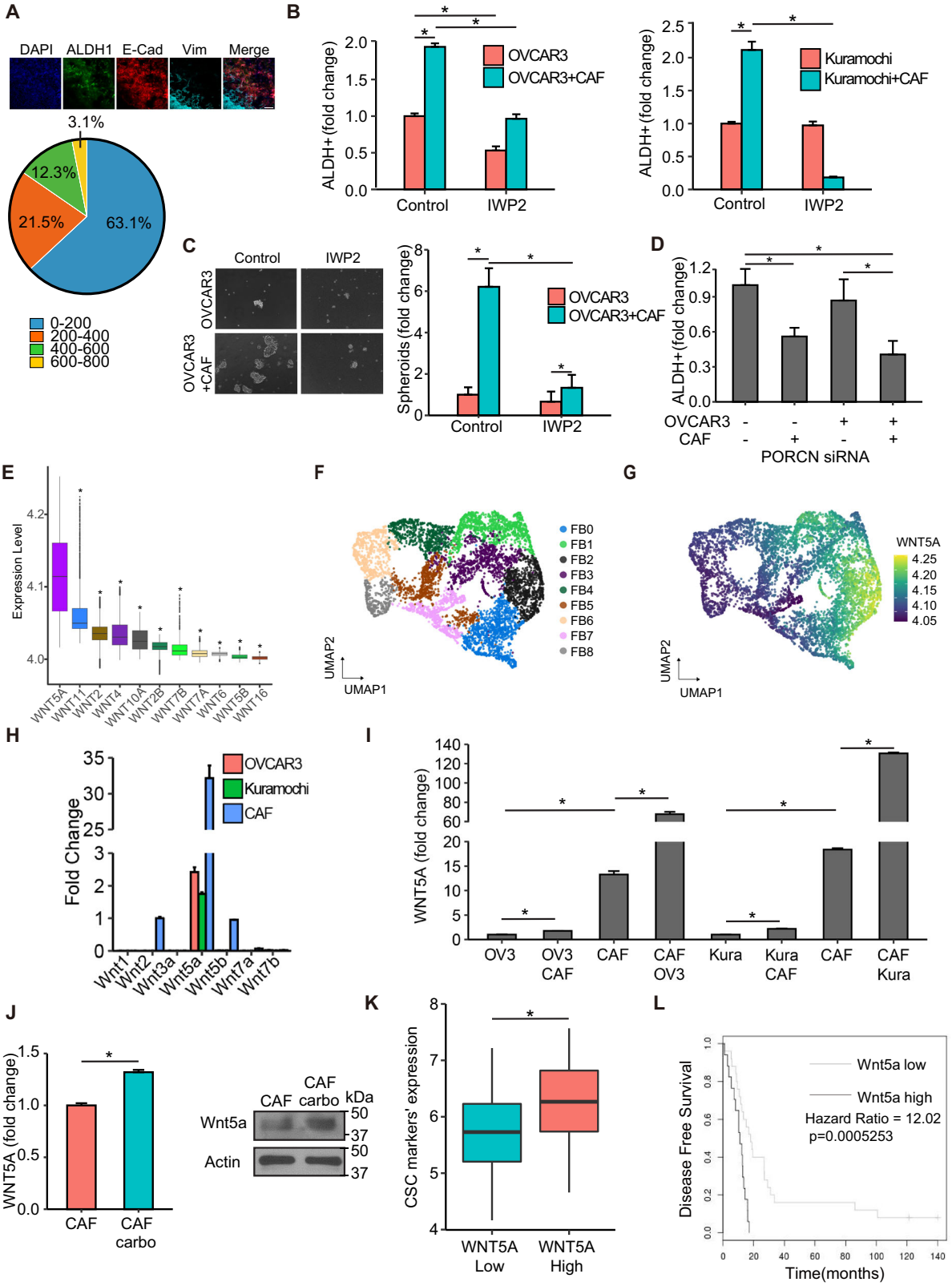

the source of the Wnt and both cancer cells and CAFs were the recipients (Fig. 5A, CC0-12, and FB0-8). To identify the signaling induced in OC cells by Wnt5a secreted by CAFs, OC cells were transfected with Super 8x TOPFlash or FOPFlash plasmids[37] and then cocultured with CAFs. Coculture with CAFs did not induce or inhibit luciferase activity, indicating that the CAFs do not influence canonical Wnt signaling in OC cells (Supplementary Fig. 8D). Similarly, treatment of OC cells transfected with the reporter/control plasmids with recombinant human Wnt5a did not affect luciferase activity, while as expected, Wnt3a induced it

Fig. 3 CAFs interact with OCSCs via Wnt signaling. A Interface interaction assay of OVCAR3 cocultured with CAFs. OVCAR3 cells and CAFs were seeded on 10 mm coverslips separated by a cloning ring. The ring was removed after 24 h and cells were allowed to grow and merge at the interface. CSCs, cancer cells, and CAFs were labeled with ALDH1 (green), E-cadherin (red), and vimentin (teal), respectively. *Top:* Images of immunofluorescence staining of OVCAR3 cells cocultured with CAFs (Leica SP8, 10x objective). *Bottom:* The distance (μm) between OCSCs and nearest CAFs in the interface interaction assay was measured by ImageJ and plotted as % of OCSCs at increasing distances from CAFs. Scale bar: 200 μm. **B** ALDEFLUOR assay for stem cell enrichment in OC-CAF coculture with IWP2. OVCAR3/Kuramochi cells were seeded with CAFs and cocultured for a week with 5 μM PORCN inhibitor IWP2. ALDEFLUOR assay was performed to label CSCs (green). Flow cytometry analysis was done to quantify CSCs in control/CAF cocultured groups. Mean ± SD from three independent experiments. *$p < 0.01$ (*t*-test). **C** Spheroid formation assay of OC-CAF coculture with PORCN inhibition. OVCAR3/Kuramochi cells were seeded with/without CAFs in ultra-low adhesion plates and cocultured for 14 days with 5 μM PORCN inhibitor IWP2. Representative images (scale bar: 400 μm) and quantifications of the number of spheroids are shown. Mean ± SD from three independent experiments. *$p < 0.01$ (t-test). **D** Knockdown of PORCN in OC/CAF: Scrambled negative control (-) or PORCN siRNA (+) was transfected in OVCAR3/CAF 48 h before coculture as indicated. OVCAR3/CAF were then cocultured for a week. ALDEFLUOR assay was performed to label CSCs (green). CSCs were quantified by ImageJ counting. Mean ± SD from three independent experiments. *$p < 0.01$ (*t*-test). **E** scRNA-seq data from 11 HGSOC patient tumors was analyzed for the expression of WNT genes in the CAFs. The boxplot represents imputed expression level of WNT genes in all CAFs. **F** UMAP plot of CAFs from scRNA-seq of 11 HGSOC patient tumors revealing their heterogeneity. The 9 CAF subpopulations (FB0-FB8) are color coded as shown. **G** UMAP plot of the CAFs, colored by WNT5A expression levels as indicated by the scale bar. **H** qPCR for Wnt expression levels in OVCAR3/Kuramochi cells and CAFs. **I** qPCR for Wnt5a expression level in OVCAR3/Kuramochi alone, CAF alone or following coculture with each other. OVCAR3 (OV3), Kuramochi (Kura) cells were cocultured for 7 days with CAFs followed by FACS isolation and qPCR for Wnt5a. Mean ± SD from three independent experiments. *$p < 0.01$ (*t*-test). **J** qPCR and immunoblotting for Wnt5a expression in CAFs treated with carboplatin. Mean ± SD from three independent experiments. *$p < 0.01$ (*t*-test). **K** Patients ($n = 285$) in the AOCS dataset (GSE9891) were ranked according to WNT5A expression as $WNT5A^{high}$ (top quartile) and $WNT5A^{low}$ (bottom quartile). Average expression of CSC markers (ALDH1A1, NANOG, SOX2, PROM1, and KIT) in $WNT5A^{high}$ and $WNT5A^{low}$ specimens was calculated and plotted. *$p < 0.01$ (*t*-test). **L** Wnt5a survival analysis from OVMARK[34]. Only serous ovarian cancer patients receiving platinum treatment were included in the analysis (GSE30161, $n = 42$). Hazard score = 12.02 on 1df, $p = 0.0005253$, FDR = 0.040.

(Supplementary Fig. 8E). Moreover, there was no change in unphosphorylated β-catenin in $ALDH^+$ vs. $ALDH^-$ OVCAR3 cells (Fig. 5B, Supplementary Fig. 12). Similarly, treatment with recombinant human Wnt5a or coculture with CAFs did not change the levels of unphosphorylated β-catenin, while inducing ALDH1 expression (Fig. 5C, D, Supplementary Fig. 12). Taken together, our data indicates that CAFs do not induce OCSCs through canonical Wnt signaling. Therefore, we checked the role of non-canonical Wnt signaling factors like PKC, CaMKII, Jun, and CREB1 in OCSC induction. Increased PKC phosphorylation was observed in $ALDH^+$ OVCAR3 cells as well as in OVCAR3 cells treated with Wnt5a or cocultured with CAFs (Fig. 5B–D). Similarly, CREB1 was phosphorylated in OCSCs and induced by Wnt5a treatment or CAF coculture (Fig. 5B–D, Supplementary Fig. 12). However, there was no effect on CAMKII and Jun (Supplementary Fig. 8F). Treatment of OVCAR3 cells with the PKC inhibitor, staurosporine, resulted in decreased ALDH activity as well as spheroid formation, indicating the role of PKC activation in OCSC induction (Fig. 5E, F, Supplementary Figs. 9A, B and 11). Staurosporine treatment also inhibited CREB1 phosphorylation and abrogated Wnt5a-induced CREB1 activation (Fig. 5G, Supplementary Fig. 12). Conversely, treatment with the PKC agonist, tetradecanoyl phorbol acetate (TPA), induced CREB1 phosphorylation, demonstrating that PKC activation phosphorylates CREB1 (Fig. 5H, Supplementary Fig. 12). CREB1 knockdown resulted in decreased OCSC induction as evidenced by inhibition of ALDH activity and spheroid formation (Fig. 5I, J, Supplementary Figs. 9C, D, and 11).

ROR2 is the key receptor mediating the CAF-OCSC crosstalk

Wnt5a can signal via frizzled receptors along with coreceptors like ROR1, ROR2, LRP5, and LRP6[33,35,38,39]. Since there are ten mammalian frizzled family members, we focused instead on identifying the specific coreceptor(s) responsible for Wnt5a-mediated OCSC induction. Only LRP5/6 and ROR2 were expressed in OVCAR3 cells (Supplementary Fig. 9E), so we knocked them down to identify the relevant coreceptor. Knocking down ROR2 inhibited ALDH activity (Fig. 6A, B, Supplementary Figs. 9F and 11) and had an even stronger effect on OVCAR3 spheroid formation (Fig. 6C). Thereafter, OVCAR3 cells were separated into $ROR2^+$ and $ROR2^-$ populations by FACS. $ROR2^+$ cells had higher ALDH1A1 expression and had an increased ability to form spheroids, indicating an enrichment of OCSCs (Fig. 6D, E). The $ROR2^+$ OVCAR3 cells had higher baseline levels of phosphorylated PKC and CREB1, which were further induced by Wnt5a, while $ROR2^-$ cells were not responsive to Wnt5a treatment (Fig. 6F, Supplementary Fig. 12). Taken together, our data indicates that ROR2 is the key receptor involved in the Wnt5a-mediated induction of OCSCs.

Combination of carboplatin and Wnt5a inhibition is effective

The residual tumors that survive chemotherapy in OC patients are enriched in OCSCs (Fig. 1C)[12]. Therefore, to prevent disease relapse, it is desirable to target these OCSCs in combination with chemotherapy. We first tested the potential of combining Wnt5a inhibition with carboplatin treatment in an in vitro spheroid formation assay using cocultures of CAFs and OVCAR3 cells. Treatment with the Wnt5a inhibitor, Box5, reduced spheroid formation significantly, when combined with carboplatin (Fig. 7A). Based on these results, we proceeded to test the effect of the combination treatment on OVCAR3 xenografts in vivo. OVCAR3 cells and CAFs were co-injected subcutaneously in female NSG mice and once the tumors were established, treatment was initiated (Fig. 7B). Mice were injected with 25 mg/kg carboplatin once a week and 1.6 mg/kg Box5 thrice a week. The mice were euthanized once the control tumors reached the permitted limit, tumors were isolated and weighed. While treatment with carboplatin or Box5 inhibited tumor growth, a combination of both was significantly more effective (Fig. 7C, Supplementary Fig. 10A). Tumor sections were stained for ALDH1A1 expression to study the effect of treatments on OCSCs (Fig. 7D). Similarly, the residual tumors were dissociated, and the cell suspension was used for a spheroid formation assay on ultra-low adhesion plates to assess the effect of the treatments on residual OCSCs (Fig. 7E, Supplementary Fig. 10B). While carboplatin alone increased the residual OCSCs, Box5 alone or in combination with carboplatin reduced OCSCs. Taken together, our data indicates that Wnt5a inhibition can be potentially combined with chemotherapy to effectively treat OC patients and improve their treatment outcomes. In conclusion, CAFs regulate the symmetric division of OCSCs as well as the dedifferentiation of bulk cancer cells to OCSCs through secretion of Wnt5a, which acts via its co-receptor ROR2, on neighboring cancer cells, phosphorylating PKC and CREB1 (Fig. 7F).

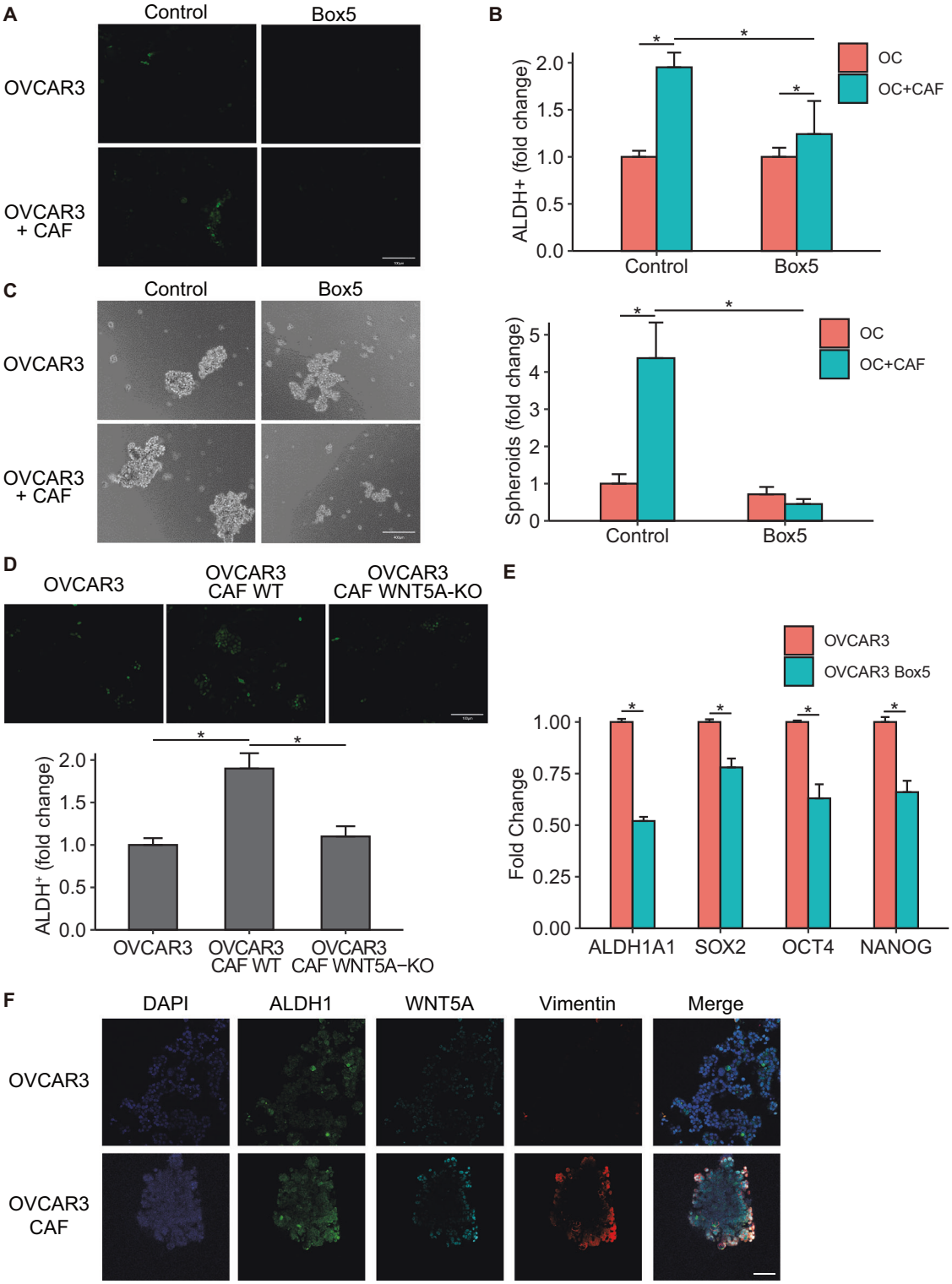

DISCUSSION

While most of the research on OC chemoresistance and OCSCs has focused on cancer cell-intrinsic mechanisms, recent reports have indicated an important role of the TME[8,40]. CAFs are a major constituent of OC TME and we have previously demonstrated the role of microRNAs in reprogramming resident normal fibroblasts into CAFs[17], while others have reported the involvement of OC extracellular vesicles in inducing CAFs[41]. CAFs have been implicated in chemoresistance and have been shown to have a role in CSC induction[42,43]. Our present findings have confirmed the role of CAFs in causing OC recurrence by providing a CSC niche. Importantly, using a novel coculture method with a defined OC-CAF boundary and regions where OC cells and CAFs are further away from each other, we have determined that CAFs have this influence only on OC cells in their proximity. This is a critical insight into the manner of the

Fig. 4 CAFs signal via Wnt5a. A, **B** ALDEFLUOR assay of OC-CAF coculture with Wnt5a inhibition. OVCAR3 cells were seeded with CAFs and cocultured for a week with 200 μM Wnt5a inhibitor Box5. ALDEFLUOR assay was performed to label CSCs (green). **A** Fluorescent imaging of OC-CAF coculture labeled by ALDEFLUOR. Scale bar: 100 μm. **B** Flow cytometry analysis was done to quantify CSCs in control/CAF cocultured groups with/without treatment. Mean ± SD from three independent experiments. *$p < 0.01$ (*t*-test). **C** Spheroid formation assay of OC-CAF coculture with Wnt5a inhibition. OVCAR3 cells were seeded with/without CAFs in ultra-low adhesion plates and cocultured for 14 days with 200 μM Wnt5a inhibitor Box5. Representative mages (left) and quantification of number of spheroids (right) are shown. Scale bar: 400 μm. Mean ± SD from three independent experiments. *$p < 0.01$ (*t*-test). **D** WNT5A was knocked out in CAFs (WNT5A-KO) using CRISPR Cas9, and the WNT5A-KO CAFs were cocultured with OVCAR3 cells followed by ALDEFLUOR assay to determine the effect on CSC. Fluorescent imaging and quantification of CSCs are shown. CSCs were quantified by ImageJ counting. Scale bar: 100 μm. Mean ± SD from three independent experiments. *$p < 0.01$ (*t*-test). **E** qPCR for CSC markers in OVCAR3 cells treated with Box5 for 3 days. Mean ± SD from three independent experiments. *$p < 0.01$ (*t*-test). **F** Immunofluorescent staining of heterotypic spheroids of OVCAR3 + CAF or OVCAR3 monoculture. OVCAR3 + CAF (1:1) were seeded in ultra-low adhesion plate for 7 days. The spheroids were isolated, fixed, and stained for respective markers. ALDH1 was labeled green, Wnt5a was labeled cyan, and vimentin (CAF marker) was labeled red. Scale bar: 200 μm.

crosstalk CAF between CAFs and OCSCs that can result in chemoresistance and relapse.

The presence of fibrotic residual lesions has been widely observed following neo-adjuvant chemotherapy in OC patients and the chemotherapy response correlates with the amount of stroma[21–23], indicating the potential role of CAFs in chemoresistance. Several mechanisms have been identified by which CAFs induce chemoresistance, including via secretion of IL-6/IL-8[44], hepatocyte growth factor (HGF)[45], and miR-522[46]. Here, we report a Wnt5a-mediated paracrine signaling mechanism that is necessary for the maintenance of OCSC population through increased symmetric division of CSCs or prevention of their differentiation and by dedifferentiation of a subpopulation of bulk OC cells. However, it is important to note that these conclusions are drawn through experimental data that do not involve direct lineage tracing. Lineage tracing experiments would be required to indisputably prove this phenomenon. Since Wnt5a is poorly soluble in the aqueous microenvironment, this signaling mechanism is limited to the immediate neighborhood. Interestingly, targeting CSCs cell-autonomous pathways is limited by the possibility of replenishment through microenvironmental signals[47]. However, targeting this crosstalk by inhibiting Wnt5a has the potential for sustained effects, as evidenced by our xenograft experiments.

The role of Wnt signaling in OCSCs has been extensively studied with a greater focus on the canonical β-catenin pathway activation[48,49]. Wnt5a has been reported to induce EMT and cancer stem cells in OC via the TGF-β1/Smad2/3 and Hippo-YAP1/TAZ-TEAD pathways[50,51]. Our analysis of published scRNA-seq data from 11 HGSOC patients[27] revealed that canonical Wnt signaling predominantly involves interactions between cancer cells in the tumor while non-canonical Wnt pathways are activated in the cancer cells by CAFs. Moreover, Wnt5a expression is the highest among all Wnts in these patient CAFs. We demonstrate that Wnt5a is important for the maintenance of OCSCs and that CAFs produce significantly greater amounts of Wnt5a than OC cells. Interestingly, Wnt5a from peritoneal mesothelial cells promotes OC metastasis[52] and high Wnt5a levels in ascites correlates with poor prognosis[53]. Mesothelial cells can be a possible source of CAFs[54] and ascites contains a significant fraction of mesothelial cells and fibroblasts that are associated with the OC cells. It is also important to note that CAFs are a heterogenous population[55–57]. Therefore, further studies are needed to determine and characterize the Wnt5a expressing CAFs that can serve as the OCSC niche. Our analysis of the scRNA-seq data from HGSOC patient metastases revealed that there are certain subpopulations of CAFs that highly express Wnt5a. Interestingly, coculture with OC cells caused an induction with Wnt5a in CAFs. This points towards an OC cell induced signaling mechanism that either increases the expression of Wnt5a in CAFs or enriches for the Wnt5a^{high} CAFs. Further studies are needed to help decipher the underlying mechanism. Treatment with carboplatin also increased Wnt5a expression in CAFs, which may involve similar mechanisms. Wnt5a affects cancer cells in a context-dependent manner, predominantly activating β-catenin independent pathways[35,58]. Our studies confirm the activation of a non-canonical Wnt signaling pathway involving ROR2/PKC/CREB1 that sustains the OCSC population. ROR2 has been implicated in OC chemoresistance and migration[59]. We further demonstrate that ROR2$^+$ OC cells are more stem-like and responsive to Wnt5a secreted by CAFs.

A phase 1 clinical trial of the porcupine inhibitor WNT974 in patients with solid tumors that have progressed despite standard therapy demonstrated that it is well tolerated[60]. Recent reports also argue in favor of targeting Wnt signaling at the ligand-receptor level[61]. Moreover, a more specific approach of inhibiting only Wnt5a is not only effective in inhibiting CSCs, as demonstrated by our in vivo experiments using Box5, but also potentially less toxic as it does not affect global Wnt signaling like a porcupine inhibitor. Therefore, developing therapies that combine Wnt5a inhibition with the standard of care carbo-taxol chemotherapy may have the potential for reducing disease recurrence in OC.

METHODS

Reagents

Cells were treated with 10 uM carboplatin (Adipogen, Cat. No. AG-CR1-3591), 200 uM Wnt5a inhibitor Box5 (Millipore Sigma, Cat. No. 681673) dissolved in pH = 7.0 $NaHCO_3$ buffer, 50 nM Staurosporine (Cell Signaling Technologies, Cat. No. 9953), 100 nM TPA (Cell Signaling Technologies, Cat. No. 4174), 10 uM IWP2 (Tocris, Cat. No. 3533) dissolved in DMSO, 200 ng/mL recombinant Human Wnt3a (R&D System, Cat. No. 5036-WN-010/CF) or Wnt5a (R&D System, Cat. No. 645-WN-010/CF) dissolved in PBS with 0.1% BSA (Fisher Scientific Cat. No. BP1600-100).

Human OC cells

Human HGSOC cell lines OVCAR3 were acquired from Ernst Lengyel at the University of Chicago and OVCAR4 was from Joanna Burdette, University of Illinois at Chicago. Kuramochi was procured from the Japanese Collection of Research Bioresources. The cell lines used were genetically validated and tested to be mycoplasma free using respective services from Idexx BioResearch (Columbia, MO). The genetic validation was done using the CellCheck 16 (16 Marker STR Profile and Inter-species Contamination Test) and mycoplasma testing was done using Stat-Myco. Epithelial OC cell lines OVCAR3, OVCAR4, OVCAR8 and Kuramochi and all CAFs were grown in DMEM media (Corning Cat. No. 10-013-CV). Media was supplemented with 10% FBS (Atlanta Biologicals Cat. No. S11150), 1% Penicillin-Streptomycin solution (100x, Corning Cat. No. 30-002-CI), 1% MEM vitamins (Corning Cat. No. 25-020-CI), and 1% MEM nonessential amino acids (Corning Cat. No. 25-025-CI). For experimental seeding or other purposes,

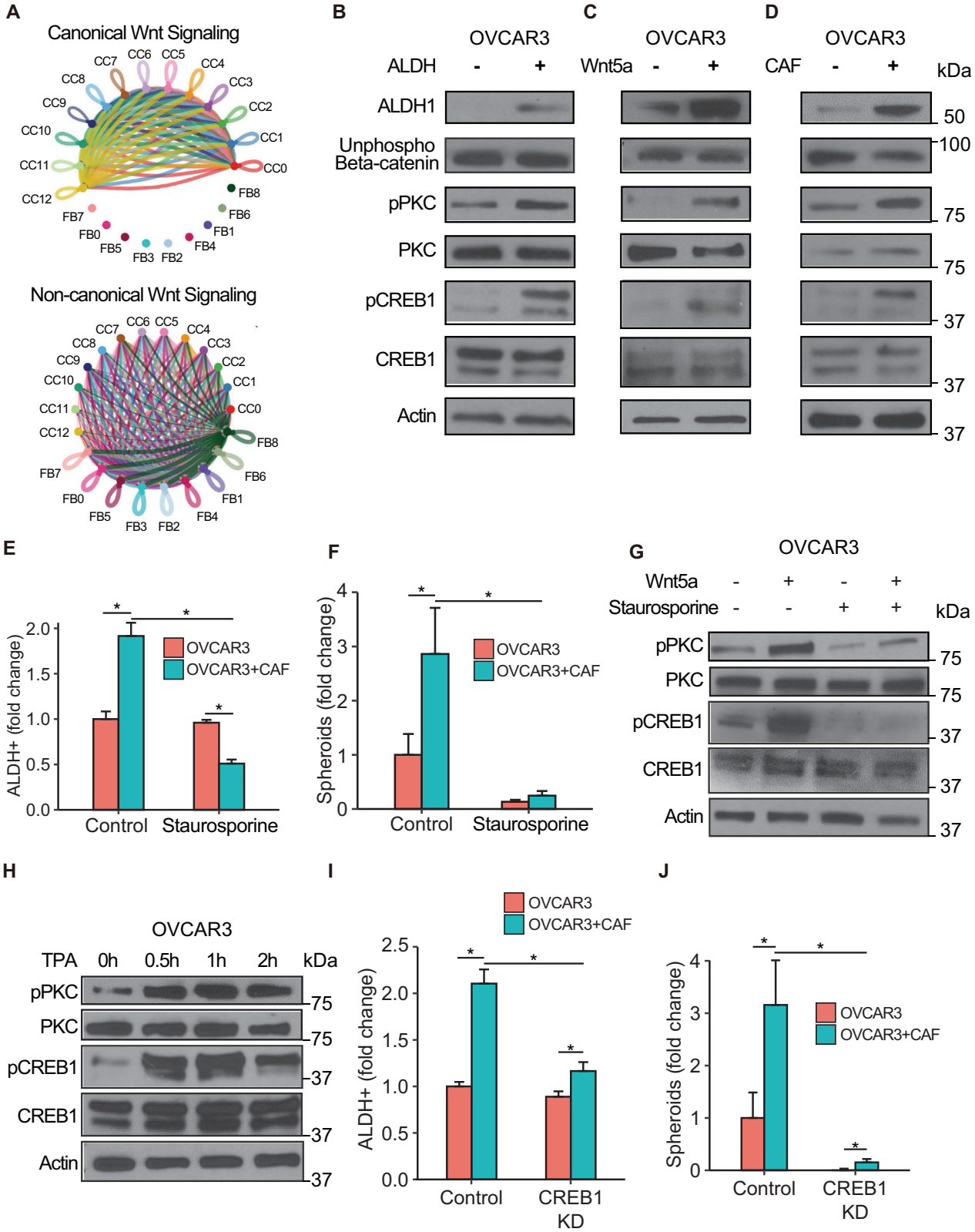

cells were detached using Trypsin EDTA 1x (Corning Cat. No. 25-053-CI). The serous OC patient ascites-derived OC cells were obtained from Dr. David Pepin, Harvard Medical School. Details of cell isolation, IBC protocol and consenting were reported previously[62]. Cells were grown in suspension culture in ultra-low attachment plates in RPMI1640 medium (Corning Cat. No. 10-040-CV) supplemented with 2% B-27 (Gibco Cat. No. 17504044) and 1% Insulin-Transferrin-Selenium (Gibco Cat. No. 41400045).

Fig. 5 Wnt5a activates PKC and CREB1. A scRNA-seq data from 11 HGSOC patient tumors was analyzed for canonical and non-canonical Wnt signaling in the cancer cell (CC0-CC12) and CAF (FB0-FB8) subpopulations using CellChat v1.5.0. The inferred canonical (top) and non-canonical (bottom) Wnt signaling network among different CC and FB subpopulations are shown. The width of line connecting nodes represent the communication probability where thicker indicates higher communication probability. Each subpopulation is represented by a specific color dot and the color of the connecting line indicates the Wnt secretor subpopulation. (CC: cancer cell; FB: CAF). **B**–**D** Immunoblot of OVCAR3 cells in different CSC conditions. ALDH1, unphosphorylated β-catenin (active), phosphorylated and total PKC, phosphorylated and total CREB1, and actin were probed. **B**: ALDEFLUOR assay was done with OVCAR3 cells, which were sorted for pure $ALDH^+$ and $ALDH^-$ cells that were lysed and used for immunoblotting. **C** OVCAR3 cells treated with 200 ng/mL Wnt5a for 2 h were lysed and used for immunoblotting. **D** OVCAR3 cells cocultured with CAFs for 7 days and isolated by FACS were lysed and used for immunoblotting. Representative blots shown from three independent experiments. **E** ALDEFLUOR assay for stem cell enrichment in OC-CAF cocultures with PKC inhibition. OVCAR3 cells were seeded with CAFs and cocultured for a week with 50 nM PKC inhibitor Staurosporine (STA). ALDEFLUOR assay was performed to label CSCs (green). Flow cytometry analysis was done to quantify CSCs in control/CAF cocultured groups with/without PKC inhibition. Mean ± SD from three independent experiments. *$p < 0.01$ (t-test). **F** Spheroid formation assay of OC-CAF coculture with Wnt5a inhibition. OVCAR3 cells were seeded with/without CAFs in ultra-low adhesion plates and cocultured for 14 days with 10 nM PKC inhibitor Staurosporine (STA). Quantification of number of spheroids are shown. Mean ± SD from three independent experiments. *$p < 0.01$ (*t*-test). **G** Immunoblot of OVCAR3 cells with Wnt5a and PKC inhibitor treatment. OVCAR3 cells were treated with 200 ng/mL Wnt5a and 50 nM Staurosporine as indicated for 2 h, followed by immunoblotting for phosphorylated and total PKC and CREB1. Representative blots shown from three independent experiments. **H** Immunoblot of OVCAR3 cells treated with PKC agonist. OVCAR3 cells were treated with 100 nM TPA for up to 2 h, followed by immunoblotting for phosphorylated and total PKC and CREB1. Representative blots shown from three independent experiments. **I** ALDEFLUOR assay for stem cell enrichment in OC-CAF cocultures with CREB1 silencing. OVCAR3 cells were transfected with CREB1 siRNA for 48 h and then seeded with CAFs and cocultured for a week. ALDEFLUOR assay was performed to label CSCs (green). Flow cytometry analysis was done to quantify CSCs in control/CAF cocultured groups with/without CREB1 silencing. Mean ± SD from three independent experiments. *$p < 0.01$ (*t*-test). **J** Spheroid formation assay of OC-CAF coculture with CREB1 silencing. OVCAR3 cells were transfected with CREB1 siRNA for 48 h and then seeded with/without CAFs in ultra-low adhesion plates and cocultured for 14 days. Representative images and quantification of number of spheroids are shown. Scale bar: 400 μm. Mean ± SD from three independent experiments. *$p < 0.01$ (*t*-test).

CAFs/fibroblasts

Human primary CAFs were isolated from freshly obtained human serous ovarian carcinoma specimens as described previously[17]. CAFs were characterized for αSMA and Vimentin expression and the absence of pan-Keratin expression by immunostaining using αSMA, Vimentin, and pan-Keratin antibodies (Cell Signaling Technologies, Cat. Nos. 19245S, 5741S, and 4545S respectively). Since the experiments involve 7-day cocultures with OC cells followed by ALDEFLUOR assay for OCSCs, it was important to distinguish the CAFs from OC cells. Therefore, CAFs were immortalized with stable expression of human telomerase reverse transcriptase (pBABE-neo-hTERT was a gift from Bob Weinberg (Addgene plasmid # 1774; http://n2t.net/addgene:1774; RRID:Addgene_1774)) and infected with lentivirus for stable RFP expression (GenTarget Inc Cat. No. LVP582). It is specified in the text wherever primary cultures of non-immortalized CAFs were used for experiments. Normal omental fibroblasts were isolated from normal human omentum obtained from female donors as described previously[17]. All specimens were de-identified human tissues that were collected during surgery by the Indiana University Simon Cancer Center's Tissue Procurement & Distribution Core using an IRB approved protocol (IRB # 1106005767). All relevant ethical regulations including the Declaration of Helsinki were complied with and written informed consent was obtained from all human participants by the core. The de-identified specimens were obtained from the core using an institutionally approved 'non-human subjects research protocol' (Protocol # 1606070934).

CAF-OC coculture

For all coculture experiments the CAFs were seeded with OC cells at a ratio of 2:1 and allowed to grow for 7 days, unless specified otherwise. Since CAFs grow at a slower rate than the OC cells, the seeding of larger number of CAFs was found to compensate for this during the period of coculture.

Bioinformatics analysis

OC patient RNA sequencing data and patient clinical features were obtained from The Cancer Genome Atlas (TCGA, https://www.cancer.gov/tcga). Microarray data of the Australian Ovarian Cancer Study (AOCS) were downloaded from the GEO database (GSE9891). The oligo (version 1.54.1) R package was used to normalize the expression matrix from the AOCS dataset. Microenvironment Cell Populations-counter (MCP-counter, version 1.2.0) was applied to deconvolve cells in TCGA and the AOCS dataset.

Analysis of scRNA-seq data

Preprocessing scRNA-seq data. Cellular annotation file and count matrix (filtered) were downloaded from GSE165897[27]. Stromal cells, immune cells, and epithelial ovarian cancer cells are identified based on cellular annotation file provided. In order to remove patient-specific effects, we ran Seurat v4.2.1 integration workflow (https://satijalab.org/seurat/articles/integration_introduction.html) for all cells to derive integration matrix by selecting 8000 features.

Imputation of scRNA-seq data. Considering the high dropout rate in single-cell sequencing data matrix, Rmagic v2.0.3 (Markov Affinity-based Graph Imputation of Cells)[63] was utilized to impute missing values, thus restoring the structure of data. We imputed gene expression using MAGIC ($k = 20$, $t = 3$) and integration matrix.

Annotation. We used the shared nearest neighbor (SNN) modularity optimization–based clustering from Seurat v4.2.1 for initial clustering. SingleR v1.10.0 was used to annotate subpopulations of stromal part of all cells and all stromal cells labeled as fibroblasts. To avoid misclassification of mesothelial and endothelial cells as fibroblasts, we used markers for mesothelial cells (CALB2, KRT19) and endothelial cells (PECAM1, THBD). Fibroblast subpopulations were isolated from stromal part for further downstream analysis workflow described in the tutorial (https://satijalab.org/seurat/articles/pbmc3k_tutorial.html) except for normalizing step to get 9 fibroblast subpopulations with resolution of 0.5. The same workflow was applied to epithelial ovarian cancer cells to get 13 cancer cell subpopulations.

Data visualization. To visualize cell layouts, uniform manifold approximation and projection (UMAP) was generated based on first 30 principal components. Imputed expression levels of different WNT variants were compared in fibroblasts and ranked from highest to lowest based on mean values in boxplot.

To visualize gene expression projected on cell layouts, imputed expression levels of WNT5A were assigned to corresponding cells in UMAP. Imputed expression levels of WNT5A were compared in

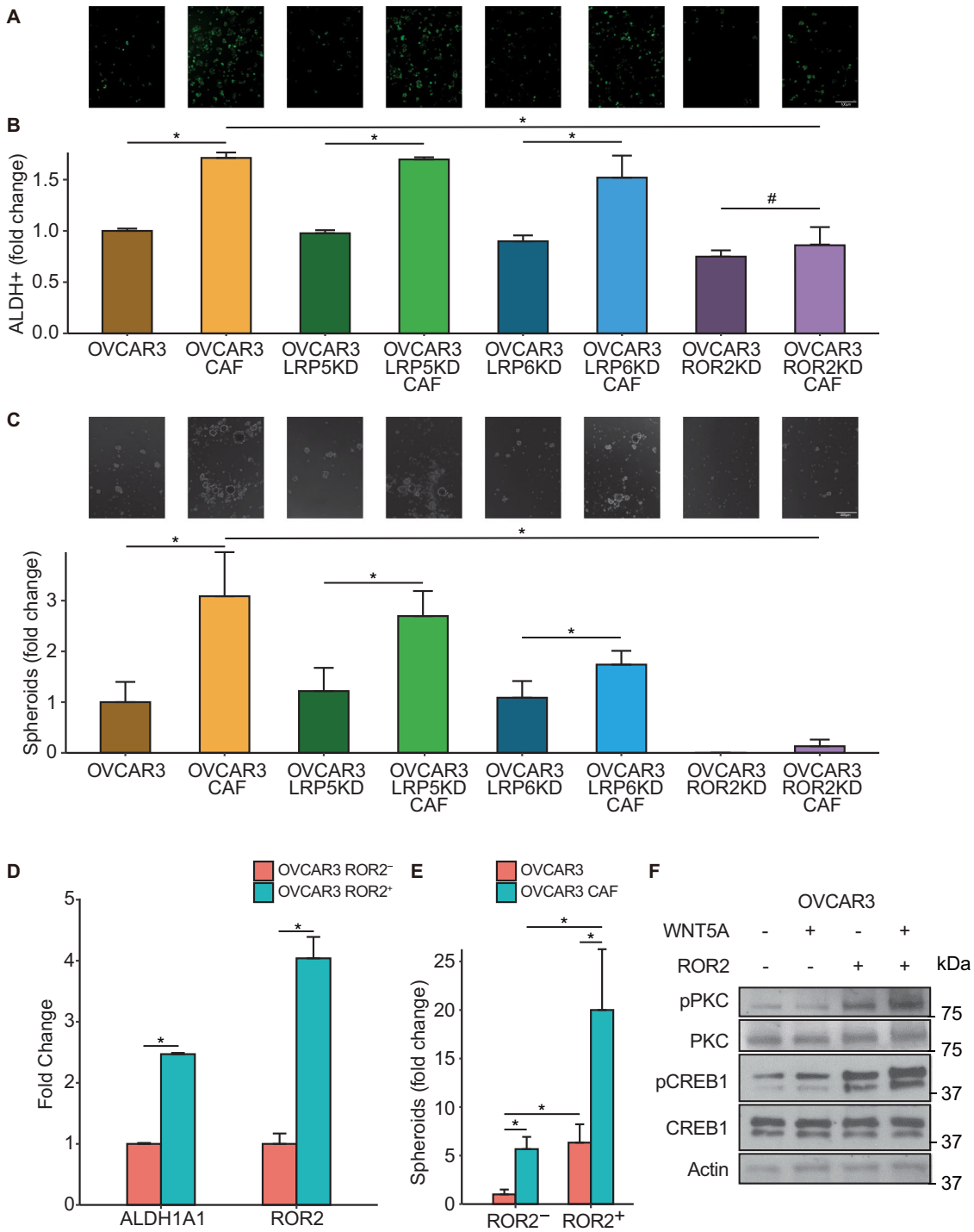

different fibroblast subpopulations in boxplot. All visualization methods were implemented in ggplot2 v3.4.0 (https://ggplot2.tidyverse.org).

Cellular communication analysis. To identify the interactions between fibroblasts and cancer cells in terms of non-canonical/canonical WNT signaling pathways, CellChat v1.5.0[36] was used to infer cell-cell communication probabilities based on imputed matrix. The workflow we used was outlined in the tutorial (https://htmlpreview.github.io/?https://github.com/sqjin/CellChat/blob/master/tutorial/CellChat-vignette.html).

ALDH enzymatic activity assay

ALDH enzymatic activity was measured using an ALDEFLUOR kit (STEMCELL Technologies Cat. No. 01700) following the manufacturer's instructions. Fluorescent imaging of the ALDEFLUOR assay was done using an EVOS FL Auto microscope (Thermo Fisher Scientific). At least 3 different images were taken from 3 different technical replicates, and at least 3 different biological replicates were done for each experiment. ALDH positive cells population was also quantified by LSRII flow cytometer (BD Biosciences) in the non-RFP cells in cocultures of OC cells with RFP expressing CAFs as outlined in Supplementary Fig. 4A. The FACS data analysis

Fig. 6 ROR2 is the Wnt5a co-receptor. A, **B** ALDEFLUOR assay for stem cell enrichment in OC-CAF cocultures with Wnt5a co-receptor inhibition. OVCAR3 cells were transfected with LRP5/LRP6/ROR2 siRNA for 48 h and then seeded with CAFs and cocultured for a week. ALDEFLUOR assay was performed to label CSCs (green). **A** Fluorescent imaging of OC-CAF coculture labeled by ALDEFLUOR. Scale bar: 100 µm. **B** Flow cytometry analysis was done to quantify CSCs in control/CAF cocultured groups. Mean ± SD from three independent experiments. * p < 0.01 # not significant (t-test). **C** Spheroid formation assay of OC-CAF cocultures with Wnt5a co-receptor inhibition. OVCAR3 cells were transfected with LRP5/LRP6/ROR2 siRNA for 48 h and then seeded with/without CAFs in ultra-low adhesion plates and cocultured for 14 days. Representative images and quantification of number of spheroids are shown. Scale bar: 400 µm. Mean ± SD from three independent experiments. *$p < 0.01$ (*t*-test). **D** qPCR for ALDH1A1 expression in $ROR2^-/ROR2^+$ OVCAR3 cells. OVCAR3 cells were sorted to isolate ROR2 negative and positive cells using FACS with a ROR2-APC conjugated antibody. Cells were lysed for RNA extraction. qPCR was done to determine ALDH1A1 and ROR2 expression. Mean ± SD from three independent experiments. *$p < 0.01$ (*t*-test). **E** Spheroid formation assay of $ROR2^-/ROR2^+$ OVCAR3 cocultured with CAFs. OVCAR3 cells were sorted to isolate ROR2 negative and positive cells using FACS with a ROR2-APC conjugated antibody. Cells were cocultured with CAFs in ultra-low adhesion plates for 14 days to form spheroids. Spheroids were quantified and plotted. Mean ± SD from three independent experiments. *$p < 0.01$ (*t*-test). **F** Immunoblots of $ROR2^-/ROR2^+$ OVCAR3 treated with Wnt5a. OVCAR3 cells were sorted using FACS to isolate ROR2 negative and positive cells using a ROR2-APC conjugated antibody. Cells were seeded in culture plate and starved for 24 h with serum-free media before treatment with 200 ng/mL Wnt5a for 2 h followed by lysis and immunoblotting. Representative blots shown from three independent experiments.

workflow and all FACS data is provided in the supplementary data file (combined in Supplementary Fig. 11). Of note, the CAFs did not have ALDH activity. In experiments to separate the ALDH positive and negative OC cells, ALDEFLUOR assay was followed by cell sorting using FACS Aria II (BD Biosciences). As an additional confirmation, RFP expressing OVCAR3 cells were cocultured with nonfluorescent CAFs followed by ALDEFLUOR assay and quantification of ALDH + OVCAR3 cells (Supplementary Fig. 4E).

Spheroid formation and imaging

Cancer cells were trypsinized and seeded in 24 well ultra-low attachment plates (Corning Cat. No. 3473) for spheroid formation assay. Cancer stem cell media is used in the assay, as described previously[4]. 1000 cells were seeded in each well and cultured for 14 days to allow spheroid formation, which were imaged using an EVOS FL Auto microscope (Thermo Fisher Scientific). At least three different images were taken from three different technical replicates, and at least three different biological replicates were done for each experiment. Spheroids were manually quantified.

Spheroid immunofluorescent staining

3×10^5 OVCAR3 cells were seeded with 3×10^5 CAFs in 6-well ultra-low attachment plates (Corning Cat. No. 3471). At the time of seeding, the plate was kept inclined for 30 min to help the OC cells and CAFs aggregate and interact. Thereafter, plates were reverted to the usual horizontal position and cultured for 7 days to allow the heterotypic spheroids to grow. Spheroid fixation, blocking, and antibody staining were done as described by Condello et al.[49]. Briefly, spheroids were fixed and permeabilized in suspension for 3 h at 4 °C in PBS containing 4% PFA (Boston BioProducts BM-155) and 1% Triton X-100 (Thermo Scientific Cat. No. 85112). Spheroids were dehydrated with increasing concentrations of methanol (25%, 50%, 75%, 95%, 100%) and rehydrated in the opposite sequence, then stained with ALDH1 (1:100, BD Bioscience Cat. No. 611194), Wnt5a (1:200, CST Cat. No. 2530) and Vimentin (1:500, Thermo Fisher Scientific Cat. No. PA1-10003) antibodies. Nuclei were visualized by Hoechst 33342 (Life Technologies Cat. No. H3570). The primary antibodies were probed with 1:1000 Alexa Fluor 488 conjugated anti-mouse IgG (Cell Signaling Technology, cat. No. 4408S), Alexa Fluor 594 conjugated anti-rabbit IgG (Cell Signaling Technology, cat. No. 8889) or Alexa Fluor 647 conjugated anti-chicken IgG (Invitrogen, cat. No. A-21449).

Interface interaction assay

OVCAR3 cells and CAFs were trypsinized and counted. 12 mm round coverslips (TED PELLA, Cat. No. 26023) were placed in wells of 24-well tissue culture plates (Corning, Cat. No. 09-761-146). Cloning rings (6 mm diameter, 8 mm height, PYREX, Cat. No. CLS31666) were carefully placed at the center of the coverslip. 15,000 OVCAR3 cells suspended in 100 µL cell culture medium were slowly added to the center of the cloning ring. 150,000 CAFs in 500 µL cell culture medium were added outside the ring in the well. After overnight incubation to allow attachment, the rings were removed. The two cell types were allowed to grow and merge at the interface over 48 h. Thereafter, cells were treated with 33 µM carboplatin (IC_{50} for MTT assay) for 48 h followed by TUNEL staining. For the ALDH1 staining experiment, cells were fixed and stained 48 h after merger at the interface. Cells were stained with ALDH1 (1:100, BD Bioscience Cat. No. 611194), E-cadherin (1:1000, Cell Signaling Technology Cat. No. 3195), and Vimentin (1:1000, Thermo Fisher Scientific Cat. No. PA1-10003) primary antibodies. Nuclei were visualized by Hoechst 33342 (Life Technologies Cat. No. H3570). The primary antibodies were probed with 1:1000 Alexa Fluor 488 conjugated anti-mouse IgG (Cell Signaling Technology, cat. No. 4408S), Alexa Fluor 594 conjugated anti-rabbit IgG (Cell Signaling Technology, cat. No. 8889) or Alexa Fluor 647 conjugated anti-chicken IgG (Invitrogen, cat. No. A-21449). Click-iT TUNEL Alexa Fluor Imaging Assay for Microscopy (Thermo Fisher Scientific Cat. No. C10245) was used according to the manufacturer's protocol to image apoptotic cells.

Tumor immunofluorescence staining

De-identified HGSOC patient tumors collected during surgery by the Indiana University Simon Cancer Center's Tissue Procurement & Distribution Core were obtained from the core using an institutionally approved 'non-human subjects research protocol' (Protocol # 1606070934). Freshly collected tumors were embedded in OCT compound (Tissue-Tek Cat. No. 4583), flash-frozen, and stored at −80 °C. 12 µm tumor sections were made using a cryo-microtome (Leica CM1850), fixed with 4% PFA for 15 min at 37 °C, permeabilized with 1X Proteinase K solution (provided in the Click-It TUNEL Assay kit) followed by TUNEL staining using Click-iT TUNEL Alexa Fluor Imaging Assay for Microscopy (Thermo Fisher Scientific Cat. No. C10245). The OC cells were labeled with Pan-Keratin (1:200, Cell Signaling Technology, Cat. No. 4545S) and CAFs with αSMA (1:200, Cell Signaling Technology, Cat. No. 19245 S). Alexa Fluor 594 conjugated goat-anti-mouse (1:1000, Cell Signaling Technology, Cat. No. 8890S) and Alexa Fluor 647 conjugated goat-anti-rabbit (1:1000, Cell Signaling Technology, Cat. No. 4414S) were used to detect the primary antibodies and nuclei were labeled with Hoechst 33342 (1:10,000, Life Technologies Cat. No. H3570). The slides were mounted with ProLong Gold (Invitrogen Cat. No. P36930), and the images were acquired with a Leica SP8 confocal microscope.

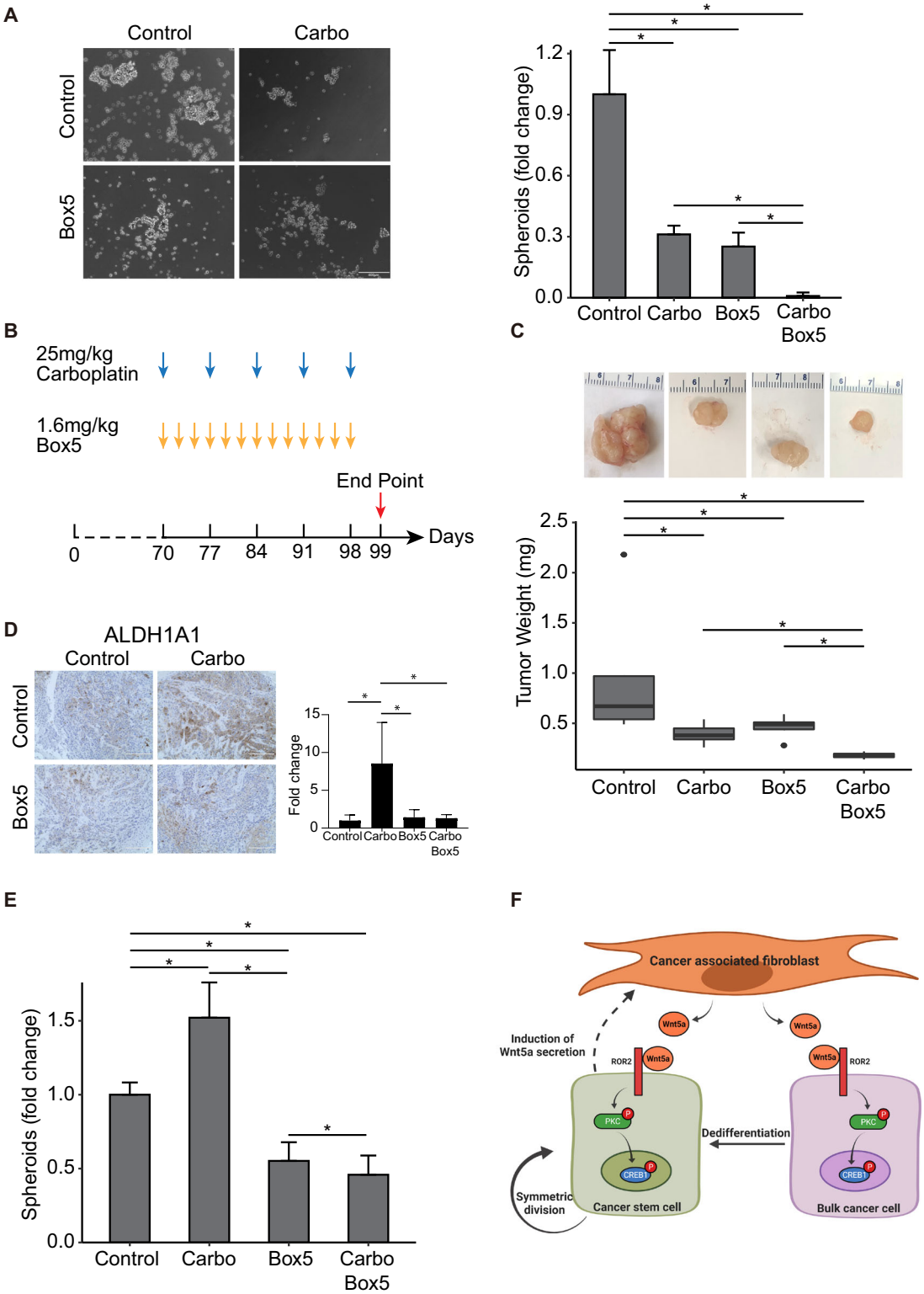

Gene silencing

Cells were seeded in culture plates in antibiotic-free DMEM one day before transfection of siRNA. Cells were transfected with 25 nM LRP5, LRP6, ROR2, CREB1 and PORCN siRNA (Dhramacon, SMARTPool Cat. Nos. L-003844-00-0005, L-003845-00-0005, L-003172-00-0005, 003619-00-0005, L-009613-00-0005 respectively) using TransIT-X2 transfection reagent (Mirus, Cat. No. MIR6003) following the manufacturer's protocol. The cells were used for experiments 48 h after transfection unless indicated otherwise.

CRISPR knockout

WNT5A sgRNA (Synthego CRISPRevolution sgRNA EZ Kit, Seq: uccugggcuuaauauuccaa) and Cas9 enzyme (Synthego Cas9 2NLS) ribonucleoprotein complexes were made following

Fig. 7 Wnt5a inhibition sensitizes tumors to carboplatin. A In vitro spheroid formation of OVCAR3-CAF cocultures with Box5/carboplatin combination treatment. OVCAR3 cells were seeded with CAFs in ultra-low adhesion plates and cocultured for 14 days with/without 200 μM Box5 and/or 10 nM carboplatin. Representative images and quantification of number of spheroids are shown. Scale bar: 400 μm. Mean ± SD from three independent experiments. *$p < 0.01$ (t-test). **B**–**E** In vivo combination treatment of Box5/carboplatin in mouse xenografts. **B** Mice were subcutaneously injected with 1 million OVCAR3+2million CAFs. When tumor size reached 1 cm in diameter (on day70 of injection), mice were randomized into 4 groups of 5 mice per group and treated with 25 mg/kg carboplatin weekly or 1.6 mg/kg Box5, three times per week or a combination of both. The control group received PBS. **C** Mice were euthanized after 4 weeks of treatment and tumors were isolated, weighted, and plotted. **D** Representative IHC Images of the xenograft tumor sections stained with ALDH1A1 (scale bar: 200 μm). ALDH1A1 staining was quantified and plotted. Mean ± SD from five tumors/group. *$p < 0.05$. **E** Residual tumors were dissociated using a gentleMACS dissociator and used for spheroid formation assay to measure the residual OCSC fraction. The spheroids were imaged and quantified. Mean ± SD from five tumors/group. *$p < 0.01$ (t-test). **F** Schematic overview of the Wnt5a-ROR2-PKC-CREB1 axis mediating the CAF-OCSC interactions.

manufacturer's protocol. The reaction mixture was electroporated into cells using NeonTransfection System 10 μL Kit (Thermo Fisher Scientific, Cat. No. MPK1025) with the Neon Transfection System (Thermo Fisher Scientific, Cat. No. MPK5000). Knockout efficiency was screened using T7E1 assay, and target protein expression level was further screened and validated by immunoblotting.

Reverse transcription-quantitative PCR

Reverse Transcription was done using MultiScribe Reverse Transcriptase kit (Thermo Fisher Scientific, Cat. No. 4311235) according to the manufacturer's protocol using a Veriti 96-Well Thermal Cycler (Thermo Fisher Scientific). Quantitative real-time PCR for ALDH1A1, Wnt5a, SOX2, OCT4, NANOG, and PORCN was performed using TaqMan gene expression assay (Applied Biosystems, Cat. Nos. Hs00946916_m1, Hs00998537_m1, Hs01053049_S1, Hs00999634_gh, Hs02387400_g1, Hs00224508_m1 respectively) using GAPDH (Applied Biosystems, Cat. No. Hs99999905_m1) as an endogenous control on LightCycler 96 PCR system (Roche) using Faststart Essential DNA master mix (Roche, Cat. No. 06924492001).

Immunoblotting

Immunoblotting was done as previously described ref. [17,64]. Briefly, electrophoresis was performed to separate proteins on 4–20% SDS-PAGE precast gels (Bio-Rad, Cat. No. 4561094) and transferred onto nitrocellulose membranes (Cytiva Amersham Cat. No. 10600002), blocked with 5% skim milk, and probed with ALDH1 (BD biosciences, Cat. No. 611194), unphosphorylated-β-catenin, pan phosphorylated-PKC, Wnt5a, pan-Keratin, phosphorylated-Jun, phosphorylated-CAMKII (Cell signaling Technologies, Cat. Nos. 19807S, 9371S, 2530S, 4545S, 3270S, 12716S respectively), phosphorylated-CREB1, pan PKC, CREB1 (Santa Cruz, Cat. Nos. sc-81486, sc-7769, sc-377154 respectively) primary antibodies (all at 1:1000 dilution) and detected using HRP-conjugated Mouse/Rabbit IgG secondary antibodies (Cell Signaling Technologies, Cat. Nos. 7076/7074) at 1:2000 dilution. β-actin-HRP antibody (Sigma, Cat. No A3854) was used to detect actin. The full images of the blots are provided in Supplementary Fig. 12. All blots in a figure derive from the same experiment and were processed in parallel.

Immunohistochemistry

Immunohistochemical experiments and Masson's Trichrome staining were performed by the Immunohistochemistry core facility of Indiana University School of Medicine using 5 μm thick formalin-fixed deparaffinized sections as previously described ref. [17,64]. Tumor sections were probed with ALDH1A1 (Abcam, Cat. No. ab52492) or αSMA (Cell Signaling Technologies, Cat. No. 19245). Images were acquired using EVOS FL Auto microscope (Thermo Fisher Scientific) using a 20x objective. OpenCV Python package was used to quantify the positive regions in the slides and implemented in Python (v3.8.3). Images were read and converted from BGR to HSV color space. The range for different regions in the images were set up and used to threshold the images to get binary values. The percentage of the positive regions for each image was calculated as the ratio of the number of non-zero pixels to the total pixels.

Xenograft experiments

OVCAR3 cells (1×10^6) and CAFs (2×10^6) were mixed in 100 μL growth factor reduced matrigel (Corning, Cat. No CLS356231) and injected subcutaneously into flanks of 6-week-old, female NSG mice. The mice were housed in special Indiana University Laboratory Animal Resources facility for immune compromised mice, with 12-h day/night cycles. Once tumors were palpable, mice were randomly segregated into 4 treatment groups ($n = 5$). Each group was treated with either carboplatin, Box5, both, or vehicle. Carboplatin (25 mg/kg) was injected i.p. once a week, Box5 (1.6 mg/kg) was injected i.p. thrice a week. PBS wa uses as the vehicle control and injected i.p. thrice a week. After 4 weeks of treatment, mice were euthanized with CO_2, followed by cervical dislocation. Tumors were removed, weighed, and dissociated with a gentleMACS Dissociator (Miltenyi Biotec) using human tumor dissociation kit (Miltenyi Biotec Cat. No. 130-095-929) for subsequent experiments. For in vivo limiting dilution assay pre-cocultured or control OVCAR3 cells were injected subcutaneously in the right and left flanks, respectively of 6-week-old female NSG mice as indicated in Fig. 2D. Mice were euthanized 71 days after injection and the tumor take was quantified. The study was approved by Indiana University's Bloomington Institutional Animal Care and Use Committee.

Study approval

All specimens were collected during surgery, having obtained informed consent prior to participation, by the Indiana University Simon Cancer Center's Tissue Procurement & Distribution Core using an IRB approved protocol (IRB # 1106005767). The de-identified specimens were obtained from the core using an institutionally approved 'non-human subjects research protocol' (Protocol # 1606070934). All animal experiments were conducted following protocols approved by the Indiana University Bloomington Institutional Animal Care and Use Committee.

Statistics

Statistical analyses were conducted using Student's *t* test. A two-tailed Student's *t*-test was used for comparison between 2 groups. For all experiments, at least three independent biological replicates ($n = 3$) were done. Mean ±SD was shown for each bar graph. *P* values of less than 0.01 were considered to be statistically significant, unless specified in the figure legend.

Reporting summary

Further information on research design is available in the Nature Research Reporting Summary linked to this article.

DATA AVAILABILITY

Publicly available scRNA-seq data was downloaded from GSE165897 for analysis.

Received: 28 March 2023; Accepted: 5 December 2023;
Published online: 08 January 2024

REFERENCES

1. Siegel, R. L., Miller, K. D., Fuchs, H. E. & Jemal, A. Cancer statistics, 2022. *CA Cancer J. Clin.* **72**, 7–33 (2022).
2. Bowtell, D. D. et al. Rethinking ovarian cancer II: reducing mortality from high-grade serous ovarian cancer. *Nat. Rev. Cancer* **15**, 668–679 (2015).
3. Vaughan, S. et al. Rethinking ovarian cancer: recommendations for improving outcomes. *Nat. Rev. Cancer* **11**, 719–725 (2011).
4. Wang, Y. et al. IL-6 mediates platinum-induced enrichment of ovarian cancer stem cells. *JCI Insight* **3**, https://doi.org/10.1172/jci.insight.122360 (2018).
5. Nacarelli, T. et al. NAMPT inhibition suppresses cancer stem-like cells associated with therapy-induced senescence in ovarian cancer. *Cancer Res.* **80**, 890–900 (2020).
6. Qian, J. et al. Cancer-associated mesothelial cells promote ovarian cancer chemoresistance through paracrine osteopontin signaling. *J. Clin. Invest.* **131**, https://doi.org/10.1172/jci146186 (2021).
7. Pietilä, E. A. et al. Co-evolution of matrisome and adaptive adhesion dynamics drives ovarian cancer chemoresistance. *Nat. Commun.* **12**, 3904–3904 (2021).
8. Batlle, E. & Clevers, H. Cancer stem cells revisited. *Nat. Med.* **23**, 1124–1134 (2017).
9. Hwang, W. L. et al. MicroRNA-146a directs the symmetric division of Snail-dominant colorectal cancer stem cells. *Nat. Cell Biol.* **16**, 268–280 (2014).
10. de Sousa e Melo, F. et al. A distinct role for Lgr5(+) stem cells in primary and metastatic colon cancer. *Nature* **543**, 676–680 (2017).
11. Li, S. S., Ma, J. & Wong, A. S. T. Chemoresistance in ovarian cancer: exploiting cancer stem cell metabolism. *J. Gynecol. Oncol.* **29**, e32 (2018).
12. Steg, A. D. et al. Stem cell pathways contribute to clinical chemoresistance in ovarian cancer. *Clin. Cancer Res.* **18**, 869–881 (2012).
13. Sansone, P. et al. Evolution of cancer stem-like cells in endocrine-resistant metastatic breast cancers is mediated by stromal microvesicles. *Cancer Res.* **77**, 1927–1941 (2017).
14. Taniguchi, S. et al. Tumor-initiating cells establish an IL-33-TGF-β niche signaling loop to promote cancer progression. *Science* **369**, https://doi.org/10.1126/science.aay1813 (2020).
15. Yeung, T. L. et al. TGF-β modulates ovarian cancer invasion by upregulating CAF-derived versican in the tumor microenvironment. *Cancer Res.* **73**, 5016–5028 (2013).
16. Gao, Q. et al. Heterotypic CAF-tumor spheroids promote early peritoneal metastatis of ovarian cancer. *J. Exp. Med.* **216**, 688–703 (2019).
17. Mitra, A. K. et al. MicroRNAs reprogram normal fibroblasts into cancer-associated fibroblasts in ovarian cancer. *Cancer Discov.* **2**, 1100–1108 (2012).
18. Richards, K. E. et al. Cancer-associated fibroblast exosomes regulate survival and proliferation of pancreatic cancer cells. *Oncogene* **36**, 1770–1778 (2017).
19. Loeffler, M., Krüger, J. A., Niethammer, A. G. & Reisfeld, R. A. Targeting tumor-associated fibroblasts improves cancer chemotherapy by increasing intratumoral drug uptake. *J. Clin. Invest.* **116**, 1955–1962 (2006).
20. Fiaschi, T. et al. Reciprocal metabolic reprogramming through lactate shuttle coordinately influences tumor-stroma interplay. *Cancer Res.* **72**, 5130–5140 (2012).
21. Lou, E. et al. Tumor-stroma proportion as a predictive biomarker of resistance to platinum-based chemotherapy in patients with ovarian cancer. *JAMA Oncol.* **5**, 1222–1224 (2019).
22. Hynninen, J. et al. Is perioperative visual estimation of intra-abdominal tumor spread reliable in ovarian cancer surgery after neoadjuvant chemotherapy? *Gynecol. Oncol.* **128**, 229–232 (2013).
23. Vergote, I. et al. Neoadjuvant chemotherapy or primary surgery in stage IIIC or IV ovarian cancer. *N. Engl. J. Med.* **363**, 943–953 (2010).
24. Tothill, R. W. et al. Novel molecular subtypes of serous and endometrioid ovarian cancer linked to clinical outcome. *Clin. Cancer Res.* **14**, 5198–5208 (2008).
25. Wang, W. et al. Dynamics between cancer cell subpopulations reveal a model coordinating with both hierarchical and stochastic concepts. *PloS One* **9**, e84654 (2014).
26. Pattabiraman, D. R. & Weinberg, R. A. Tackling the cancer stem cells - what challenges do they pose? *Nat. Rev. Drug Discov.* **13**, 497–512 (2014).
27. Zhang, K. et al. Longitudinal single-cell RNA-seq analysis reveals stress-promoted chemoresistance in metastatic ovarian cancer. *Sci. Adv.* **8**, eabm1831 (2022).
28. Carter, K., Rameshwar, P., Ratajczak, M. Z. & Kakar, S. S. Verrucarin J inhibits ovarian cancer and targets cancer stem cells. *Oncotarget* **8**, 92743–92756 (2017).
29. Brooks, M. D. & Wicha, M. S. Tumor Twitter: cellular communication in the breast cancer stem cell niche. *Cancer Discov.* **5**, 469–471 (2015).
30. Farin, H. F. et al. Visualization of a short-range Wnt gradient in the intestinal stem-cell niche. *Nature* **530**, 340–343 (2016).
31. Hayakawa, Y. et al. Mist1 expressing gastric stem cells maintain the normal and neoplastic gastric epithelium and are supported by a perivascular stem cell niche. *Cancer Cell* **28**, 800–814 (2015).
32. Arensman, M. D. et al. WNT7B mediates autocrine Wnt/β-catenin signaling and anchorage-independent growth in pancreatic adenocarcinoma. *Oncogene* **33**, 899–908 (2014).
33. Yuzugullu, H. et al. Canonical Wnt signaling is antagonized by noncanonical Wnt5a in hepatocellular carcinoma cells. *Mol. Cancer* **8**, 90 (2009).
34. Madden, S. F. et al. OvMark: a user-friendly system for the identification of prognostic biomarkers in publically available ovarian cancer gene expression datasets. *Mol. Cancer* **13**, 241 (2014).
35. Zhou, Y., Kipps, T. J. & Zhang, S. Wnt5a signaling in normal and cancer stem cells. *Stem Cells Int.* **2017**, 5295286 (2017).
36. Jin, S. et al. Inference and analysis of cell-cell communication using CellChat. *Nat. Commun.* **12**, 1088 (2021).
37. Veeman, M. T., Slusarski, D. C., Kaykas, A., Louie, S. H. & Moon, R. T. Zebrafish prickle, a modulator of noncanonical Wnt/Fz signaling, regulates gastrulation movements. *Curr. Biol.* **13**, 680–685 (2003).
38. Astudillo, P. Wnt5a signaling in gastric cancer. *Front. Cell Dev. Biol.* **8**, 110 (2020).
39. Ring, L., Neth, P., Weber, C., Steffens, S. & Faussner, A. β-Catenin-dependent pathway activation by both promiscuous "canonical" WNT3a-, and specific "noncanonical" WNT4- and WNT5a-FZD receptor combinations with strong differences in LRP5 and LRP6 dependency. *Cell. Signal.* **26**, 260–267 (2014).
40. Lenos, K. J. et al. Stem cell functionality is microenvironmentally defined during tumor expansion and therapy response in colon cancer. *Nat. Cell Biol.* **20**, 1193–1202 (2018).
41. Giusti, I. et al. Tumor-derived extracellular vesicles activate normal human fibroblasts to a cancer-associated fibroblast-like phenotype, sustaining a pro-tumorigenic microenvironment. *Front. Oncol.* **12**, 839880 (2022).
42. Zhang, D. et al. Tumor-stroma IL1β-IRAK4 feedforward circuitry drives tumor fibrosis, chemoresistance, and poor prognosis in pancreatic cancer. *Cancer Res.* **78**, 1700–1712 (2018).
43. Wang, H. et al. Rab13 sustains breast cancer stem cells by supporting tumor-stroma cross-talk. *Cancer Res.* **82**, 2124–2140 (2022).
44. Su, S. et al. CD10(+)GPR77(+) cancer-associated fibroblasts promote cancer formation and chemoresistance by sustaining cancer stemness. *Cell* **172**, 841–856.e816 (2018).
45. Deying, W. et al. CAF-derived HGF promotes cell proliferation and drug resistance by up-regulating the c-Met/PI3K/Akt and GRP78 signalling in ovarian cancer cells. *Biosci. Rep.* **37**, https://doi.org/10.1042/bsr20160470 (2017).
46. Zhang, H. et al. CAF secreted miR-522 suppresses ferroptosis and promotes acquired chemo-resistance in gastric cancer. *Mol. Cancer* **19**, 43 (2020).
47. Garber, K. Cancer stem cell pipeline flounders. *Nat. Rev. Drug Discov.* **17**, 771–773 (2018).
48. Huels, D. J. et al. Wnt ligands influence tumour initiation by controlling the number of intestinal stem cells. *Nat. Commun.* **9**, 1132 (2018).
49. Condello, S. et al. Tissue tranglutaminase regulates interactions between ovarian cancer stem cells and the tumor niche. *Cancer Res.* **78**, 2990–3001 (2018).
50. Dehghani-Ghobadi, Z., Sheikh Hasani, S., Arefian, E. & Hossein, G. Wnt5A and TGFβ1 converges through YAP1 activity and integrin alpha v up-regulation promoting epithelial to mesenchymal transition in ovarian cancer cells and mesothelial cell activation. *Cells* **11**, https://doi.org/10.3390/cells11020237 (2022).
51. Ford, C. E. et al. The non-canonical Wnt ligand, Wnt5a, is upregulated and associated with epithelial-to-mesenchymal transition in epithelial ovarian cancer. *Gynecol. Oncol.* **134**, 338–345 (2014).
52. Asem, M. et al. Host Wnt5a potentiates microenvironmental regulation of ovarian cancer metastasis. *Cancer Res.* **80**, 1156–1170 (2020).
53. Kotrbová, A. et al. WNT signaling-inducing activity in ascites predicts poor outcomes in ovarian cancer. *Theranostics* **10**, 537–552 (2020).
54. Huang, H. et al. Mesothelial cell-derived antigen-presenting cancer-associated fibroblasts induce expansion of regulatory T cells in pancreatic cancer. *Cancer Cell* **40**, 656–673.e657 (2022).
55. Friedman, G. et al. Cancer-associated fibroblast compositions change with breast cancer progression, linking the ratio of S100A4(+) and PDPN(+) CAFs to clinical outcome. *Nat. Cancer* **1**, 692–708 (2020).
56. Lavie, D., Ben-Shmuel, A., Erez, N. & Scherz-Shouval, R. Cancer-associated fibroblasts in the single-cell era. *Nat. Cancer* **3**, 793–807 (2022).
57. Wang, J. et al. Modulation of immune infiltration of ovarian cancer tumor microenvironment by specific subpopulations of fibroblasts. *Cancers* **12**, https://doi.org/10.3390/cancers12113184 (2020).

58. Asem, M. S., Buechler, S., Wates, R. B., Miller, D. L. & Stack, M. S. Wnt5a Signaling in cancer. *Cancers* **8**, https://doi.org/10.3390/cancers8090079 (2016).
59. Henry, C. E., Llamosas, E., Djordjevic, A., Hacker, N. F. & Ford, C. E. Migration and invasion is inhibited by silencing ROR1 and ROR2 in chemoresistant ovarian cancer. *Oncogenesis* **5**, e226 (2016).
60. Rodon, J. et al. Phase 1 study of single-agent WNT974, a first-in-class Porcupine inhibitor, in patients with advanced solid tumors. *Br. J. Cancer* **125**, 28–37 (2021).
61. Flanagan, D. J., Vincan, E. & Phesse, T. J. Wnt signaling in cancer: not a binary ON: OFF Switch. *Cancer Res.* **79**, 5901–5906 (2019).
62. Pépin, D. et al. AAV9 delivering a modified human Mullerian inhibiting substance as a gene therapy in patient-derived xenografts of ovarian cancer. *Proc. Natl Acad. Sci. USA* **112**, E4418–E4427 (2015).
63. van Dijk, D. et al. Recovering gene interactions from single-cell data using data diffusion. *Cell* **174**, 716–729.e727 (2018).
64. Dasari, S. et al. Signals from the metastatic niche regulate early and advanced ovarian cancer metastasis through miR-4454 downregulation. *Mol. Cancer Res.* **18**, 1202–1217 (2020).

ACKNOWLEDGEMENTS

We are deeply indebted to the patients for their generosity and to Indiana University Simon Cancer Center's Tissue Procurement & Distribution Core for collecting patient specimens. We also acknowledge the help of the Center for Genomics and Bioinformatics, Flow Cytometry Core Facility, and Light Microscopy Imaging Center at IU Bloomington as well as the Immunohistochemistry Core of IU Health. This research was supported by DoD OCRP Ovarian Cancer Academy Award (W81XWH-15-0253), American Cancer Society Research Scholar Grant (RSG-21-019-01-CSM), CTSI core pilot, and Ralph W. and Grace M. Showalter Research awards to A.K.M.

AUTHOR CONTRIBUTIONS

Y.F. was involved in experiment design. Y.F. and X.X. performed the experiments and data analysis. J.W. helped with bioinformatics analysis and did the scRNA-seq analysis. SD helped with the animal experiments. D.P., K.P.N., and D.Z. provided resources and advice in experiment design. D.Z. helped with the IHC experiments in patient specimens. A.K.M. was involved in the conception, design, supervision, analysis, and interpretation of data and manuscript preparation.

COMPETING INTERESTS

The authors declare no competing interests.

ADDITIONAL INFORMATION

Supplementary information The online version contains supplementary material available at https://doi.org/10.1038/s41698-023-00495-5.

Correspondence and requests for materials should be addressed to Anirban K. Mitra.

Reprints and permission information is available at http://www.nature.com/reprints

Publisher's note Springer Nature remains neutral with regard to jurisdictional claims in published maps and institutional affiliations.